NASA Contractor Report 4005

Convective Heat Transfer From Circular Cylinders Located Within Perforated Cylindrical Shrouds

Kamran Daryabeigi and Robert L. Ash

CONTRACT NAS1-17993
AUGUST 1986

NASA

NASA Contractor Report 4005

Convective Heat Transfer From Circular Cylinders Located Within Perforated Cylindrical Shrouds

Kamran Daryabeigi and Robert L. Ash
Old Dominion University Research Foundation
Norfolk, Virginia

Prepared for
Langley Research Center
under Contract NAS1-17993

National Aeronautics
and Space Administration

**Scientific and Technical
Information Branch**

1986

This Page Intentionally Left Blank

TABLE OF CONTENTS

This Page Intentionally Left Blank

LIST OF TABLES

This Page Intentionally Left Blank

LIST OF FIGURES

LIST OF FIGURES

LIST OF SYMBOLS

A	area
b	width of wind tunnel
°C	degrees Celsius
C_D	drag coefficient
C_p	specific heat at constant pressure
D	diameter
e	height of wind tunnel
E	error
Gr	Grashof number
h	convective heat transfer coefficient
I	current
ID	inside diameter
J	radiosity
K	degrees Kelvin
k	thermal conductivity
L	length of cylinder
ℓ	characteristic length
Nu	Nusselt number
P	pressure
Pr	Prandtl number
$\dot{Q}$	heat transfer rate
q''	heat flux
R	gas constant
Re	Reynolds number
T	temperature
U	velocity

V	voltage
X	blockage fraction
α	thermal diffusivity
ε	emissivity
θ	shroud orientation angle
μ	viscosity
ν	kinematic viscosity
ρ	density
σ	Stephan-Boltzman constant
ϕ	radius ratio
ψ	ventilation factor

Subscripts

d	dynamic
eff	effective
m	mean
R	radiative
s	surface
sh	shroud
ss	solid
st	static
w	wake
∞	free stream

1. INTRODUCTION

Experiments have been performed to investigate the convective heat transfer for transverse flow over solid cylinders located concentrically within perforated cylindrical shrouds. This work was motivated by the need for convective heat transfer data applicable to these configurations. Such data could be used in the development of response models for platinum resistance thermometers (prt's) which have similar shrouded cylinderical configurations. One of the important parameters in the response modeling of prt's is the convective heat transfer coefficient to the sensor (cylinder) [1].*

Utilization of perforated shrouds on bare cylinders can serve two purposes. First, they act as radiation shields. Perforated shrouds have also been shown to be effective in reducing vibration of cylindrical geometries caused by vortex shedding [2]. In an effort to develop ways of suppressing wind-induced oscillations of tall smokestacks, Price [3] has concluded that the enclosure of a cylinder within a concentric perforated shroud was an effective method of vibration reduction. He has also found that the drag coefficient of shrouded cylinders was approximately 0.6, and it was relatively immune to variations in Reynolds number. Walshe [4] has also reported that perforated shrouds could stabilize flow-induced oscillations around cylinders. While reducing vibrations of cylinders, shrouds tend to complicate the convective heat transfer to cylinders. The influence of these perforated shrouds on the convective heat transfer to the cylinder located concentrically inside them is the subject of this study.

No definitive heat transfer correlations for transverse flow over cylinders located concentrically inside perforated shrouds exist. Warshawsky [5] has addressed this issue, and has recommended using the shroud temper-

---

*Number in brackets represents references.

ature as the free stream fluid temperature and estimating a fluid velocity based on perforation size and internal flow impedance, in order to calculate the heat transfer coefficient for the inner cylinder. He then recommended using conventional bare cylinder heat transfer correlations for this idealized case. Those approximations have not been substantiated, and that was an additional consideration in this experimental investigation.

The convective flow through the shroud represents a formidable theoretical problem. Since patterns of circular holes are used typically to allow fluid flow to occur in the annular space between the shroud and the inner cylinder, the flow is periodic in the spanwise direction and three-dimensional. Furthermore, the presence of the ventilating holes provides pressure relief around the outer cylinder so that classical solid cylinder pressure distributions around the shroud do not occur. In fact, it is the balancing of the two pressure distributions -- one due to classical flow around cylinders and the other due to suction and blowing through the ventilation region -- that controls the two coupled flow fields. These flow fields are influenced by the following parameters:

1. Reynolds number
2. Degree of shroud ventilation
3. Shroud orientation with respect to the flow
4. The size of the flow passage between the shroud and the inner cylinder
5. Free-stream turbulence intensity
6. Aspect ratio -- length to diameter ratio of the sensor assembly
7. Perforation hole size and shape
8. Perforation hole pattern

9. Thickness of shroud
10. Surface finishes

We can define a shroud ventilation factor, ψ, as the ratio of the open area to the total surface area of the perforated portion of the shroud. The flow between the shroud and cylinder can be characterized by a radius ratio, ϕ, which is the ratio of shroud's inside radius to the radius of the inner solid cylinder, and serves as a nondimensional parameter representing the clearance between the two tubes.

It was not possible to investigate all the parameters defined here. However, the influence of Reynolds number, ventilation factor, and shroud orientation with respect to flow were studied. Some of the results were presented in an earlier publication [6]. In the continuation of this investigation it was decided to include also the influence of radius ratio, because it appeared to be a very important parameter. The present work provides comprehensive results obtained throughout this study.

In order to place the shrouded cylinder work in perspective, a brief discussion of earlier bare cylinder experiments is required. Analytical solutions of the convective heat transfer coefficient for different solid geometries require the solution of governing conservation equations (mass, momentum, and energy), and are restricted to relatively simple geometries. Convective heat transfer coefficients for most geometries, including cylinders, are evaluated from empirical relations determined by a combination of dimensional analysis and experiments.

The three most important nondimensionalized parameters for convective heat transfer correlations are: Nusselt number, Nu, which is the basic dimensionless convective heat transfer coefficient ($Nu = h\ell/k$), Reynolds

number, Re, which is the ratio of inertial to viscous forces of the fluid ($Re = \frac{U\ell}{\nu}$), and Prandtl number, Pr, which is the ratio of mechanical to thermal diffusion ($Pr = \frac{\mu C_p}{k} = \frac{\nu}{\alpha}$).

Numerous correlations for forced convection heat transfer for cylinders in cross flow exist. A summary of recent work on the mean heat transfer rates from circular cylinders is contained in a paper by Morgan [7]. Morgan has reported that the Nusselt number for a given Reynolds number varies by up to 29% for various experimental data and as much as 46% for various correlations. These large variations are caused by such factors as: experimental uncertainty, and nonsimilarity of experimental conditions (different surface roughness, free-stream turbulence intensities, etc.).

Measurements of forced convective heat transfer coefficients for cylinders can be found in papers by Hilpert [8] and Schmidt and Wenner [9]. Hilpert performed measurements on circular cylinders in a cross flow of air covering a wide range of Reynolds numbers. Schmidt and Wenner [9] have measured the variation of local heat transfer coefficients over the surface of cylinders. Giedt [10] has also measured the variation of local heat transfer coefficients over non-isothermal cylinders.

The correlation used in this investigation for the mean convective heat transfer rates from cylinders is that proposed by Morgan [7] which is the corrected form of Hilpert's correlation [8].

2. EXPERIMENTAL SET-UP

For the purpose of clarity, a typical industrial platinum resistance thermometer is shown schematically in Figure 1. It can be seen that the tip of the sensor consists of two concentric cylinders -- an inner cylinder

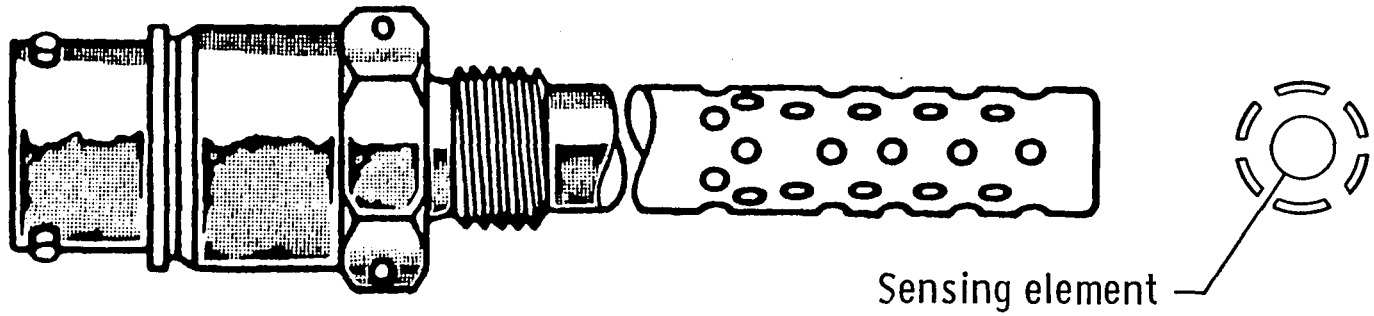

Fig. 1. Schematic diagram of a typical industrial platinum resistance thermometer.

encapsulating the resistance element, and an outer perforated cylindrical shroud fitted over the inner cylinder. That basic geometry was used in designing the present experiments.

All of the experiments in this investigation were conducted in the NASA, Langley Research Center Instrument Research Division's low speed, open circuit wind tunnel. The tunnel was manufactured by Astro Dynamics and has a test section which is 30 cm x 43 cm. The facility could be operated with flow speeds between 3.5 and 80 m/s. The wind tunnel motor could be operated at both low and high speed ranges. When the wind tunnel motor was set at the low speed range, flow velocities between 3.5 and 40 m/s could be obtained by controlling vane openings. All of the experiments in this investigation were conducted with the motor at low speed. The variation of the free-stream turbulence intensity with free-stream velocity is shown in Figure 2 for the motor set at the low speed range. The data were obtained using hot wire anemometry. The high turbulence intensities at the lowest speeds may be related to excessive instrumentation noise.

The experimental apparatus consisted of an inner cylinder, referred to as the "test cylinder" or "bare cylinder," and a set of perforated shrouds with different ventilation ratios and different diameters. A photograph of the test cylinder and some of the shrouds used in the experiment is shown in Figure 3. This figure also includes the end mounts and struts used for installing the experimental apparatus in the wind tunnel. A photograph of a shroud fitted over the inner cylinder is shown in Figure 4. A photograph of the experimental apparatus installed in the wind tunnel is shown in Figure 5. The wind tunnel and the supporting instrumentation used in this investigation are shown in Figure 6.

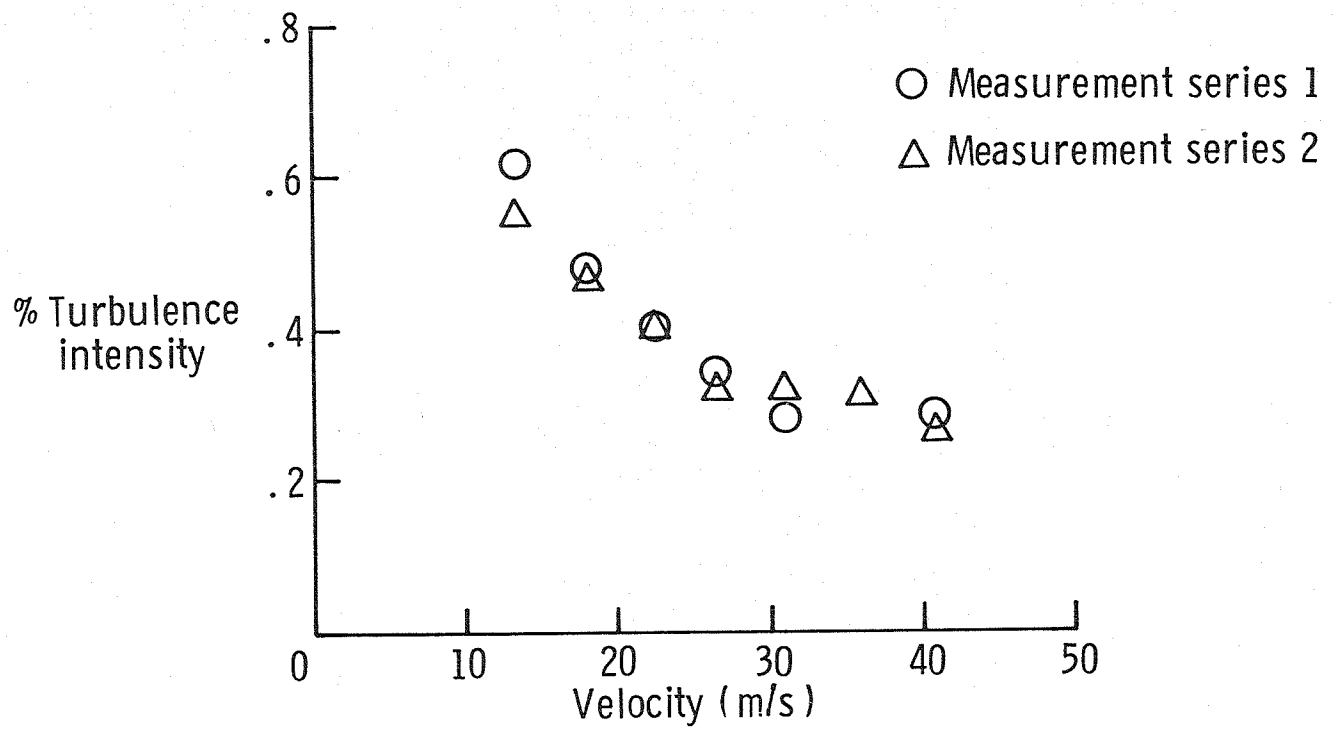

Fig. 2. Free stream turbulence intensity of wind tunnel facility at low speeds, courtesy of Debra L. Carraway, NASA Langley Research Center.

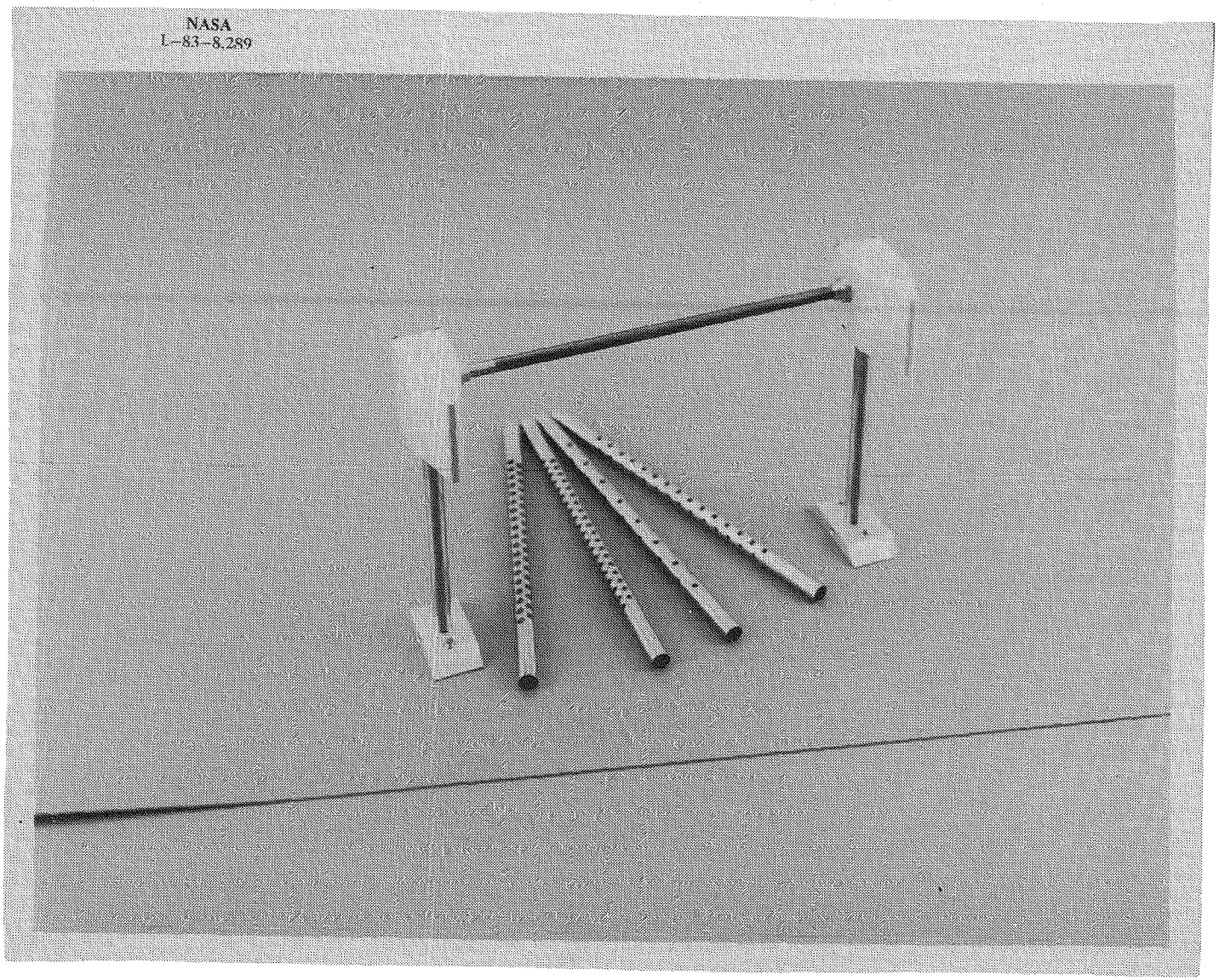

Fig. 3 Test cylinder and some representative perforated shrouds.

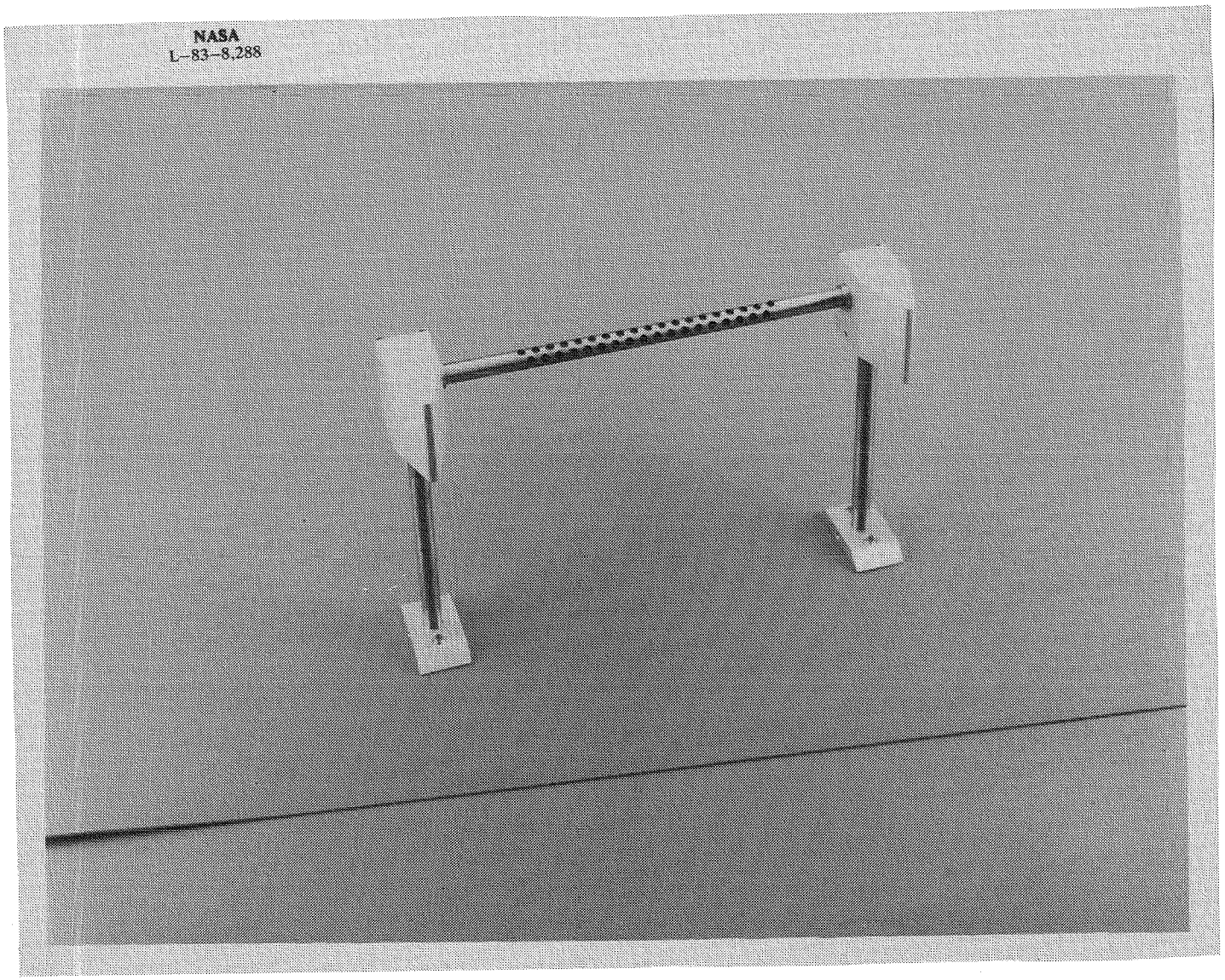

Fig. 4. A perforated shroud fitted over the bare cylinder.

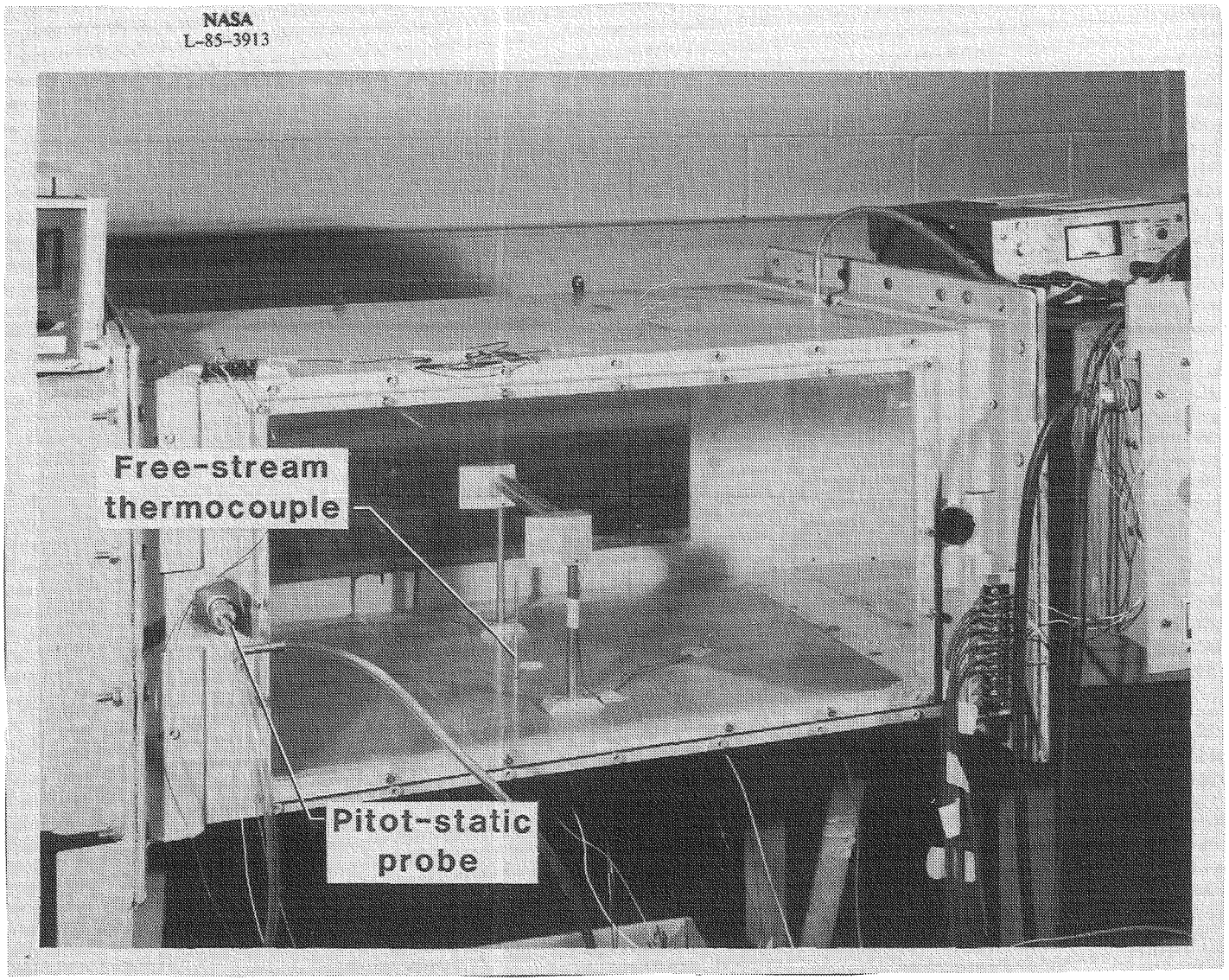

Fig. 5. Experimental apparatus installed in the wind tunnel.

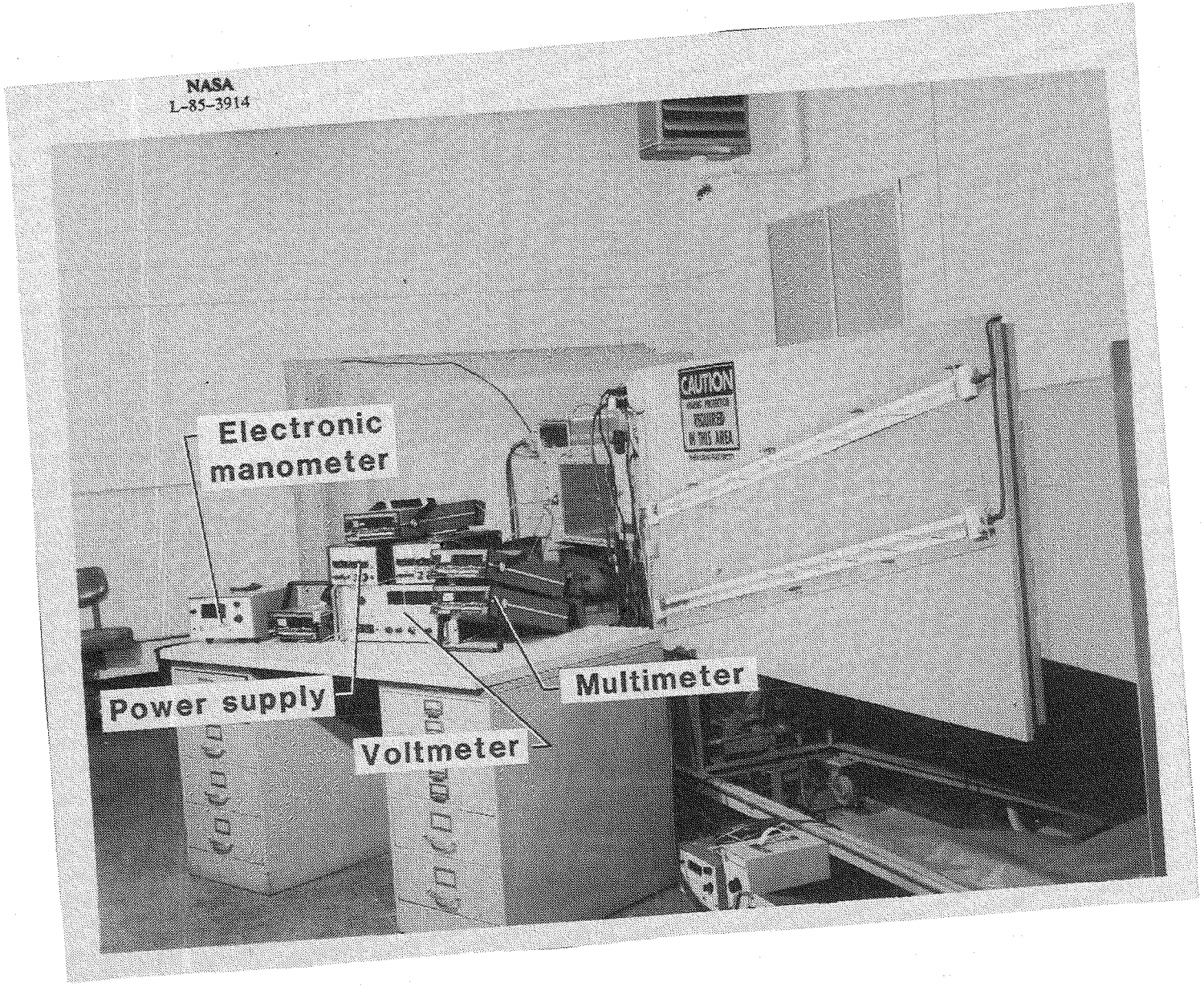

Fig. 6. Wind tunnel and related instrumentation.

2.1 Test Cylinder

A brass tube with an outside diameter of 7.9 mm and a wall thickness of 1.1 mm was used as the test cylinder throughout the experiments. Since the local heat transfer coefficient on a circular cylinder varies considerably across the surface of the cylinder [9], a good thermal conductor is required to approximate an isothermal surface. Therefore, brass, a relatively high thermal conductivity alloy, was used in order to minimize surface temperature variation (straight copper tubes with the desired outside diameter were not available). However, local temperature variations were assumed throughout the experiment.

The test cylinder had an aspect ratio (length to diameter ratio) of 26. It was decided to use the central 76.2 mm of the length of the cylinder, where longitudinal variation of temperature is negligible (refer to Appendix A), for the experimental determination of the convective heat transfer coefficient. A sectional view of the test cylinder with the specified 76.2 mm instrumented section is shown in Figure 7.

Five 0.25 mm diameter kapton insulated chromel/alumel thermocouples were mounted near the surface of the test cylinder for surface temperature measurement. The thermocouples were staggered 12.7 mm on either side of the test cylinder symmetry plane, and were located at angles of 0° (forward stagnation line), 15°, 75°, 120°, and 300° as shown in Figure 8. The thermocouple wires were drawn through the central region of the test cylinder, then out to the surface through 0.64 mm diameter holes, and soldered in place. The thermocouple junctions could not be installed exactly at the surface. It was estimated that the thermocouple junctions were located to within one wire diameter from the tube surface. Calculations showed that a position error equal to one wire diameter into the tube, would produce a

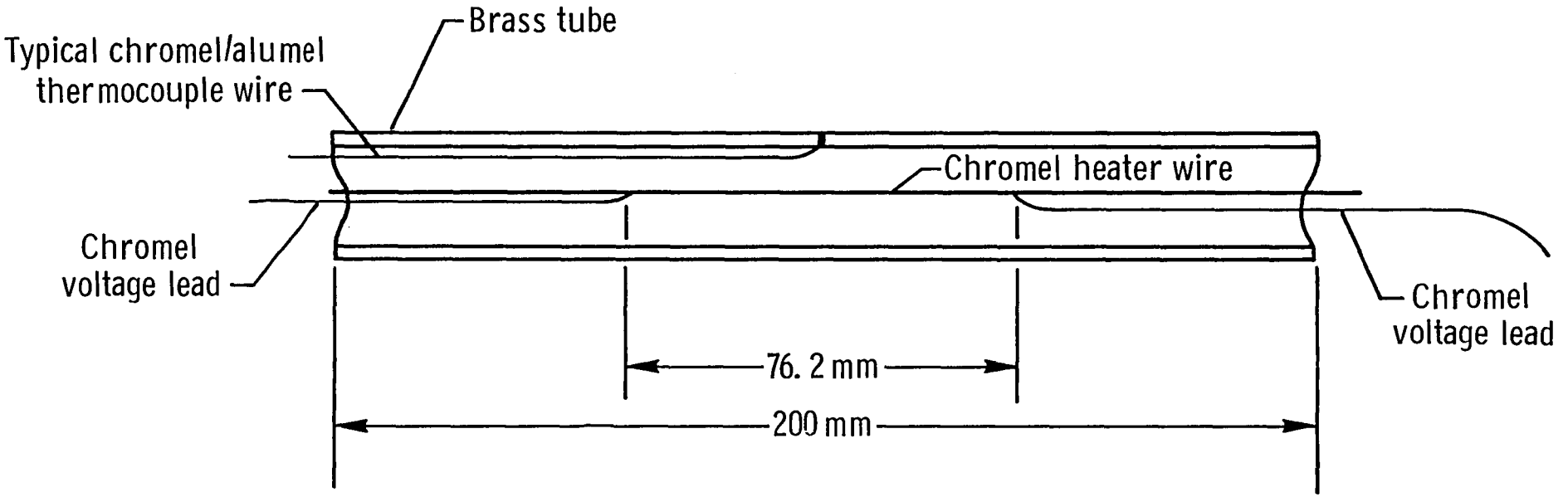

Fig. 7. Sectional view of test cylinder.

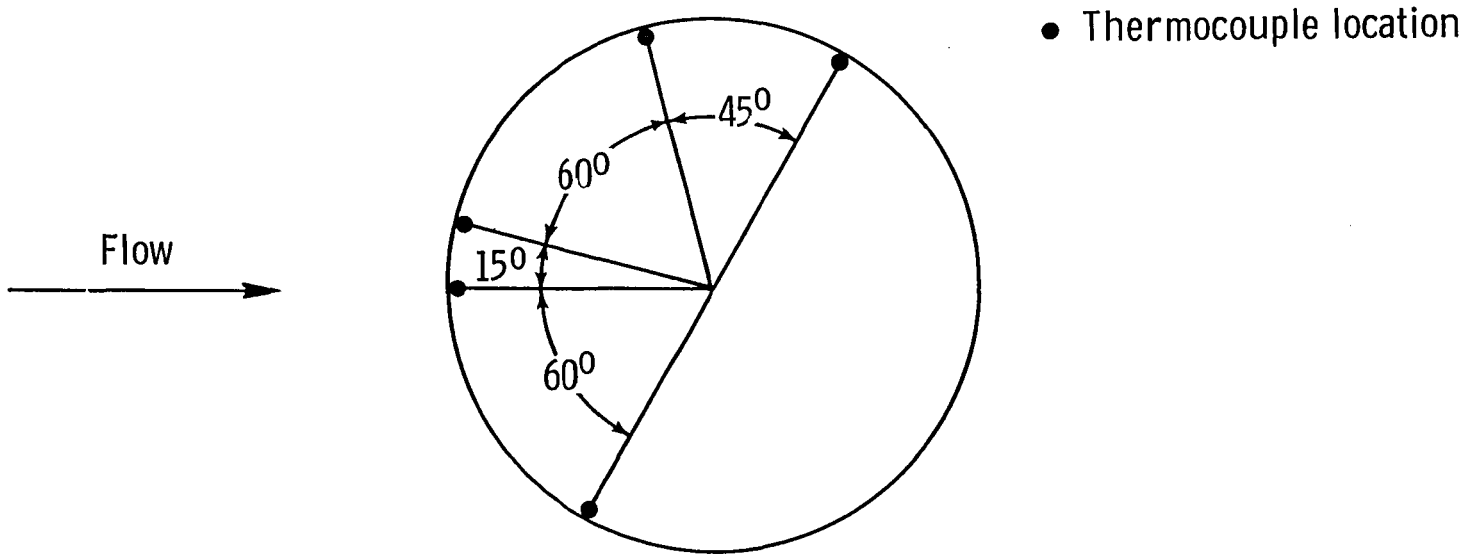

Fig. 8. Circumferential location of thermocouples on test cylinder.

measured surface temperature error of less than 0.3°C at the steady state heating rate used throughout the experiment (1040 w/m^2). That estimate was conservative since it was assumed that the thermal environment was controlled by a low thermal conductivity potting compound, rather than by the brass. The potting compound was used to fill the tube and will be described later. The general installation of a thermocouple in the test cylinder is also shown in Figure 7. During preliminary testings it was found that the thermocouple junction located at 15° was not close to the surface; therefore, measurements at that location were ignored.

An 18 gauge (1 mm diameter) chromel wire located on the axis of the test cylinder served as the heating element. The centrality of the heater wire was very important in producing uniform heating across the test cylinders. Two 0.08 mm diameter teflon insulated chromel wires were spot welded to the heater wire for measurement of the voltage drop across the central 76.2 mm of the test cylinder assembly as shown in Figure 7. Simultaneous measurements of the voltage drop across the central portion of the heater wire, and the current supplied to the heater wire were used to determine the steady state energy flow per unit length in the central portion of the test cylinder.

The heating wire, voltage leads, and thermocouples were potted in place using EpoxyLite #205 (manufactured by EpoxyLite Corp.)* which had a thermal conductivity of 0.52 W/mK for the temperature range of this experiment. The following procedure was performed for applying the potting compound:

---

*Certain commercial equipment, instruments, or materials are identified in this paper in order to adequately specify the experimental procedure. Such identifications do not imply recommendation, nor does it imply that the material or equipment identified are necessarily the best available for the purpose.

1. The test cylinder was set vertically.
2. The heating wire was set at the central axis of the tube, held in position by applying tension.
3. The top and bottom part of the tube were capped.
4. The potting compound was pumped into the tube from the bottom part using a syringe.
5. The potting compound was cured at room temperature for approximately 12 hours.

After the completed test cylinder was cured, the assembly was x-rayed to verify the position of the heater wire. It was found that the heater wire was centered to within the resolution of the x-ray picture.

2.2 Perforated Shrouds

Perforated shrouds employed on industrial platinum resistance thermometers typically have 4 to 6 rows of staggered circular holes, with ventilation factors of .15 to .20, and radius ratios between 1 and 2. Three sets of stainless steel shrouds were chosen for this investigation that would result in radius ratios of 1.1, 1.4, and 2.1 when fitted over the test cylinder. Stainless steel tubes were selected because of ease of punching the required holes on their surfaces without deforming the tubes. The dimensions of each set of shrouds are listed in Table 1. Each set consisted of

Table 1. Dimensions of test shrouds.

Nominal Radius Ratio	O.D.	Wall Thickness	Actual Radius Ratio
1.1	9.5 mm (3/8")	.25 mm (.010")	1.14
1.4	12.7 mm (1/2")	.89 mm (.035")	1.38
2.1	19.05 mm (3/4")	1.24 mm (.049")	2.09

three perforated shrouds with nominal ventilation factors of 0.09, 0.18, and 0.27. The set of perforated shrouds with radius ratio of 1.1 also included a tube with a ventilation factor of 0.36. Six rows of circular holes were drilled in the stainless steel tubes to produce the various ventilation factors. The holes were staggered in successive rows which were located at 60° intervals around the tube circumference. The ventilation factors were controlled by using different hole diameters and hole spacings. Details about the hole size, hole spacing, and total number of holes used on each perforated shroud are provided in Table 2.

Table 2. Design data for perforated shrouds.

Tube No.	Radius Ratio ϕ	Nominal Ventilation Factor ψ	Hole Diameter (mm)	Hole Spacing (mm)	Total Number of Holes	Actual Ventilation Factor
1	1.1	.09	3.2 (1/8")	18.5	45	.090
2	1.1	.18	3.2	9.0	87	.180
3	1.1	.27	3.3 (.130")	6.4	117	.263
4	1.1	.36	4.0 (5/32")	6.9	111	.359
5	1.4	.09	4.8 (3/16")	30.6	27	.091
6	1.4	.18	4.8	15.3	51	.173
7	1.4	.27	4.8	10.2	75	.254
8	2.1	.09	6.3 (1/4")	40.2	21	.083
9	2.1	.18	6.3	17.2	45	.178
10	2.1	.27	6.3	12.1	63	.250

The shroud temperature was required for calculation of radiation heat flux correction. Two 0.25 mm diameter chromel/alumel thermocouples were mounted on each shroud to measure characteristic shroud temperatures. The

thermocouples were attached to the outer surface of each shroud at nominal distances of 6.0 cm from one end of the shroud, separated by an angle of approximately 180°. That location was considered far enough from the end mount to minimize end effects, and also outside of the central instrumented section to minimize flow distortions. The thermal junctions of these thermocouples were attached to the shrouds by spot-welding the individual wires, approximately 1.6 mm apart, to the outer surface of the shrouds. This installation, which causes the metal of the shroud to become involved in the thermoelectric circuit, has proven to be satisfactory when no temperature gradients exist within the (1.6 mm) region separating the two wires [11]. Only one thermocouple was attached to each of the perforated shrouds with a radius ratio of 1.1.

2.3 Related Instrumentation

The supporting instrumentation used in this experimental investigation is described in this section. A Hewlett-Packard DC power supply (model 6267B, current range 0-10 amps) was used to provide power to the heater wire. For tests involving the perforated shrouds with radius ratios of 1.4 and 2.1, two Trygon Electronics DC power supplies (model HR60-5B, current range 0-5 amps) were used in parallel, to supply the required 5.5 amps current to the heater wire. Voltage and current applied to the heater were measured with a Dymec integrating digital voltmeter (model 2401 C), and a Fluke digital multimeter (model 8120A), respectively. Thermocouple temperature measurements were made using Joseph Kaye and Company, Inc. ice point reference standards, and the Dymec voltmeter. Wind tunnel dynamic pressure measurements were made using a Datametrics Barocel differential pressure transducer (model 570) and electronic manometer (model 1174).

3. EXPERIMENTAL PROCEDURE AND ANALYSIS

The bare cylinder correlations of Hilpert [8] have been studied by Morgan [7] and corrected using improved thermophysical property data. The correlation is in the form:

$$Nu_m = D_2 \, Re^{n_1} \qquad (1)$$

where D_2 and n_1 are the correlation constants, and are contained in Table 3 along with Hilpert's original correlation constants.

Table 3. Comparative correlation constants for convective heat transfer to cylinders (for use with Equation 1)

Hilpert's Constants				Morgan's Constants			
Re				Re			
From	To	D_2	n_1	From	To	D_2	n_1
1	4	.891	.330	1	4	*	*
4	40	.821	.385	4	35	.795	.384
40	$4x10^3$	.615	.466	35	$5x10^3$	.583	.471
$4x10^3$	$4x10^4$	.174	.618	$5x10^3$	$5x10^4$	.148	.633
$4x10^4$	$4x10^5$	.0239	.805	$5x10^4$	$2.3x10^5$	.0208	.814

*Too few data.

Both Nusselt and Reynolds numbers are based on the cylinder diameter. It should be noted that all the correlations reported here are for the special case of air, but could be extended to other fluids by multiplying the Nusselt number by the ratio of the Prandtl number of the fluid to the

Prandtl number of air raised to an appropriate power (usually 1/3).

3.1 Test Procedure

It was decided to perform the experiments for two sets of Reynolds numbers given in Table 3. The Reynolds number ranges of 35 to 5,000 and 5,000 to 50,000 were selected. The nominal Reynolds numbers used throughout the experiments were 1800, 2700, 4000, 6000, 9000, and 14000. This Reynolds number range was representative of Reynolds numbers that would occur on shrouded prt's located in the stagnation region of the National Transonic Facility at NASA Langley Research Center. Since this investigation was motivated by a need for improved response modeling of platinum resistance thermometers for that facility, that Reynolds number range was of primary interest.

It was desirable to maintain a minimum temperature difference of 5°C between the surface of the test cylinder and free stream. A simple one dimensional -- heat transfer analysis (neglecting axial variation) for the multilayered cylinder was performed, and it was found that a heater current of 5.5 amps would be sufficient to maintain the desired 5°C temperature differential at the highest Reynolds number used in this experiment. This current would correspond to a 1040 w/m^2 heat flux based on the surface area of the instrumented section of the test cylinder. This heat flux value was used throughout the experiments.

The first step in the experimental investigation consisted of measuring convective heat transfer coefficients for the test cylinder in normal flow over the Reynolds number range 1000 to 20000. The results were compared with Morgan's correlations [7] to validate the experimental procedure. Then, the experiments were repeated with the perforated shrouds fitted over

the test cylinder.

The variation of convective heat transfer with Reynolds number, ventilation factor and radius ratio of shrouds was studied. Originally, shroud orientation with respect to flow was not considered to be a primary parameter in this study, but it became apparent that this effect could not be ignored. Referring to Figure 9, it can be seen that a variety of flow fields can be created in the annular region by rotating the shroud about its axis. Defining the reference orientation as $\theta = 0°$ (case a), it can be seen that the two coupled flow fields can be altered continuously by rotating the shroud through angles of up to 30° from the reference orientation. At that point symmetry becomes a factor. In order to assess the shroud orientation variable, the three configurations tested are described briefly in Table 4. For shroud cases with radius ratios of 1.4 and 2.1, only configurations a and c ($\theta = 0°$, $\theta = 30°$) were tested.

Table 4. Shroud hole configurations (Refer to Figure 9).

Designation	Flow Angle	Comments
a	$\theta = 0°$	Symmetric, maximum pressure relief
b	$\theta = 15°$	Asymmetric, intermediate flow
c	$\theta = 30°$	Symmetric, maximum pressure difference

3.2 Surface Temperature Variation

Local heat transfer coefficient on a circular cylinder varies considerably across the surface of the cylinder [9]. This would in turn cause circumferential variation of surface temperature around the cylinder. It was desirable to consider average heat transfer coefficients in this investigation. Therefore, an average surface temperature was required in order to properly estimate the average heat transfer coefficient. One major concern

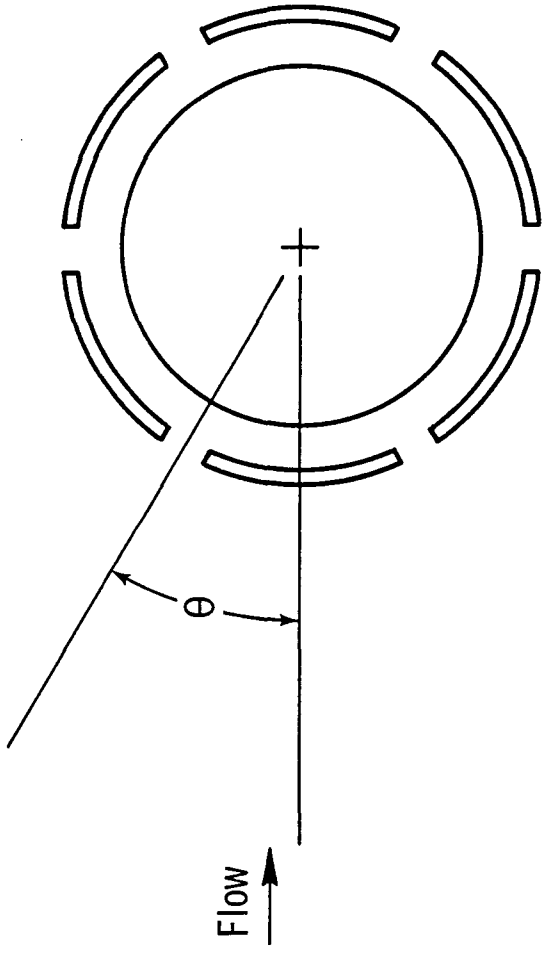

Fig. 9. Schematic diagram of shroud orientation angle.

in this analysis was whether the four surface temperature measurements around the cylinder were sufficient to yield an accurate average surface temperature. However, it was believed that the circumferential variation of surface temperature and heat transfer coefficient would be more pronounced for the bare cylinder case compared to the shrouded cylinder case. The shrouded cylinder case was believed to have a much stronger viscous coupling, a smeared stagnation region, and with flow separation occurring much further downstream compared to the bare cylinder case.

Even though a relatively high thermal conductivity tube (brass) was utilized to prevent significant surface temperature variation, further analytical investigation was required to determine maximum surface temperature variation for the limiting bare cylinder case.

Influence of the circumferential variation of heat transfer coefficient on the surface temperature of the test cylinder was studied using a two dimensional finite volume numerical model of the test cylinder. A listing of the program is presented in Appendix B. Schmidt and Wenner's [9] data for the circumferential variation of Nusselt number, for a Reynolds number of 39,800 (representative of the highest Reynolds number used in this experimental investigation), shown in Figure 10, was used in this study. It was found that the surface temperature variation would be negligible, with a maximum variation of 0.03°C under the simulated test conditions. Based on these results, it was concluded that using four surface temperature measurements around the cylinder, for calculating the average surface temperature was sufficient.

3.3 Determination of Convective Heat Transfer Coefficient

The electrical heat flux applied to the test cylinder can be related to

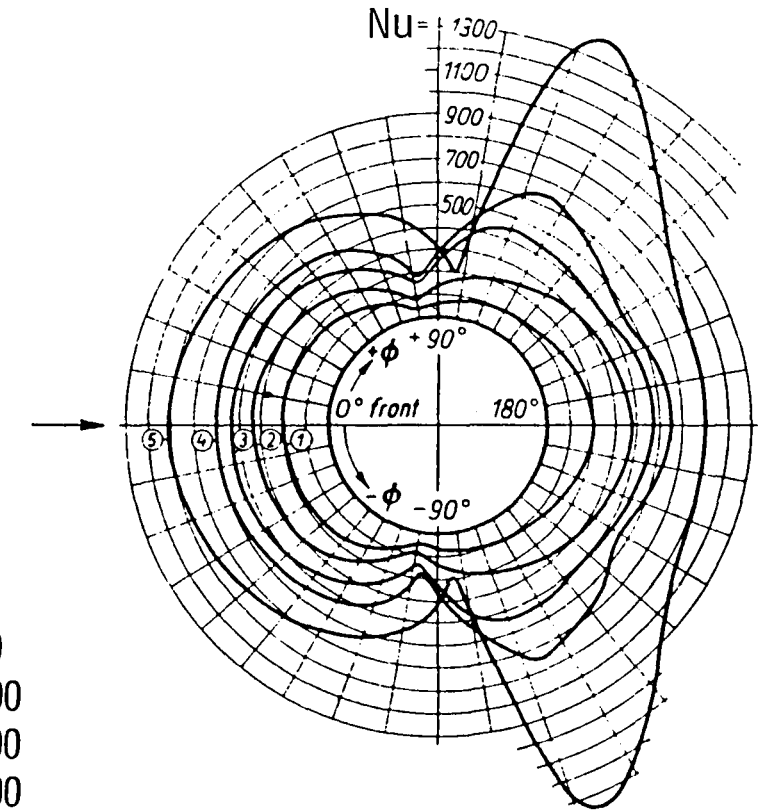

(1) Re = 39 800
(2) Re = 101 300
(3) Re = 170 000
(4) Re = 257 000
(5) Re = 426 000

Fig. 10. Circumferential variation of convective heat transfer around a cylinder, after Schmidt and Wenner [9].

the desired average heat transfer coefficient, $\overline{h}$, through Newton's law of cooling:

$$\overline{h} = (q''-q''_R)/(\overline{T}_s-T_\infty) \qquad (2)$$

where:

q'' = applied heat flux

q''_R = radiation heat flux correction

$\overline{T}_s$ = average test cylinder surface temperature

T_∞ = free-stream temperature

The simultaneous measurement of the voltage drop across the heater (V), and the current applied to the heater (I), could be used to calculate the steady-state energy flow rate in the central, instrumented section of the test cylinder ($\dot{Q} = V\ I$). The energy flow rate could be converted directly to an energy flux, q", through the outside surface of the central section of the test cylinder, which is given by:

$$q'' = \dot{Q}/\pi\ D_s L \qquad (3)$$

where D_s = diameter of test cylinder

L = length of the central instrumented section of test cylinder, 76.2 mm

The average surface temperature of the test cylinder was determined using the surface mounted thermocouples. No attempts were made to correct the measured surface temperatures for temperature field distortions caused by

the presence of the thermocouples. Free-stream temperatures were measured with a 0.25 mm diameter kapton insulated chromel/alumel thermocouple located in the wind tunnel stream, 2.5 cm upstream and 7.6 cm below the axis of the test cylinder. Upper and lower wind tunnel surface temperatures were also measured using 0.25 mm diameter kapton insulated chromel/alumel thermocouples in order to check for flow stratification. Maximum temperature differences of 1°C were observed between the upper and lower walls. The stratification effects were neglected throughout the analysis. However, the wind tunnel wall temperature measurements were used in the calculation of a radiation heat flux correction for the bare cylinder cases.

For the case of the bare cylinder, gray body, non-participating medium assumptions were used to estimate the radiation exchange between the test cylinder and the wind tunnel walls. The corresponding radiation heat flux correction was:

$$q''_R = \frac{\varepsilon}{1 - \varepsilon} [J_1 - \sigma \overline{T}_S^4] \qquad (4)$$

where:

ε = total emissivity of test cylinder

σ = Stephan-Boltzman constant

J_1 = radiosity of the test cylinder

The derivation of the above equation from the basic governing laws of radiation heat transfer, and the calculation of the test cylinders radiosity are contained in Appendix C. The outside surface of the test cylinder was coated with silver acrylic lacquer (with a measured total emissivity of 0.36) so that the radiation heat exchange with the surroundings could be estimated accurately.

Estimation of radiation correction for the case of shrouded cylinders proved to be more difficult, since the test cylinder would exchange radiation with the perforated shroud, and the wind tunnel walls through the perforations on the shroud. The shroud would also exchange radiation with the wind tunnel walls. Exact radiation modeling of this problem was formidable and excessively time consuming. Consequently, two different approximate methods were used:

1. Neglect the presence of the shroud, and consider radiation exchange only between the bare cylinder and the wind tunnel walls.
2. Consider the shroud to be unperforated, thus assuming radiation exchange between two infinitely long concentric cylinders with gray surfaces through non-participating medium.

It was found that both approximations produced comparable results. The maximum radiation heat flux (at the lowest Reynolds number) amounted to less than 5% of the applied I^2R heat flux. It was decided to use the second approximate method for calculating the radiation correction. The corresponding correction was calculated [12] according to:

$$q''_R = \frac{\sigma(\overline{T}_s^4 - \overline{T}_{sh}^4)}{1 + \frac{1-\varepsilon}{\varepsilon} + \frac{D_s(1-\varepsilon_{sh})}{ID_{sh}\,\varepsilon_{sh}}} \qquad (5)$$

where:

ε_{sh} = total emissivity of shroud

ID_{sh} = shrouds inside diameter

$\overline{T}_{sh}$ = average shroud temperature

The heat transfer coefficients obtained from Equation 2 were converted into Nusselt number data through:

$$Nu = \frac{h\ D_s}{k} \tag{6}$$

where k is the thermal conductivity of airstream. All the thermophysical properties for the airstream were evaluated using dry air tables [13] at the mean temperature, T_m, as suggested by Eckert [14]:

$$T_m = \frac{T_\infty + \overline{T}_s}{2} \tag{7}$$

The experimental Nusselt numbers were compared with Morgan's correlations [7] for cylinders in normal flow as given by Equation 1. The Reynolds numbers were calculated using

$$Re = \frac{U\ D_s}{\nu} \tag{8}$$

where:

U = free-stream velocity

ν = kinematic viscosity of airstream

The free-stream velocities were calculated using Bernoulli's equation:

$$U = \sqrt{\frac{2 P_d}{\rho}} \tag{9}$$

where:

ρ = airstream density

P_d = dynamic pressure

Dynamic pressures were measured using a pitot-static tube located in the test section of the wind tunnel, 30 cm ahead of the test cylinder. The free-stream density was calculated using the ideal gas equation:

$$\rho = \frac{P_{st}}{R\,T} \tag{10}$$

where:

R = gas constant for airstream

P_{st} = static pressure

Factors which complicate experimental heat transfer investigations are: wind tunnel blockage, free-stream turbulence intensity, and natural convection. These factors have been examined, and are addressed subsequently.

3.3.1 Flow Blockage Effects

The flow interference by the model and its supports in wind tunnel testing causes the velocity at the location of the model to be higher than the undisturbed wind tunnel speed. Two of the most important components of this interference are:

1. Solid blockage which causes an increase in the axial velocity at the model location due to a reduction in the cross sectional flow

area of the wind tunnel. Growth of the wind tunnel wall boundary layer also causes small increases in the free stream velocity.

2. Wake blockage which is similar to solid blockage, but is caused by the reduction of speed in the wake of the model. That reduced speed wake causes the mass flow rate to increase outside of the wake to maintain conservation of mass.

Blockage is usually expressed in terms of a blockage factor, X, defined by [15]:

$$U_F = U\ (1 + X) \tag{11}$$

where U is the undisturbed tunnel speed and U_F is the speed in the tunnel at the position of the model. Different forms of solid and wake blockage corrections exist [7]. The solid blockage fraction, X_{ss}, for a cylinder spanning the width of a closed rectangular tunnel, and located at a distance, β, from the tunnel axis can be estimated [16] by:

$$X_{ss} = 0.822\ \left(1 + \frac{3\ \pi^2}{4}\ \frac{\beta^2}{e^2}\right)\ \left(\frac{D}{e}\right)^2 \tag{12}$$

where e represents the height of the tunnel. The corresponding wake blockage factor, X_w, can be estimated [17] by:

$$X_w = \frac{1}{4}\ \frac{D}{e}\ C_D \tag{13}$$

where C_D is the drag coefficient. It is usual to assume that the correc-

tions are independent and simply additive [15], so the total blockage factor, X, for a cylinder with length, ℓ, is:

$$X = \frac{\ell}{b} \{0.822 \left(1 + \frac{3\pi^2}{4} \frac{\beta^2}{e^2}\right) \left(\frac{D}{e}\right)^2 + \frac{1}{4} \left(\frac{D}{e}\right) C_D\} \qquad (14)$$

where

b = width of tunnel

The total blockage for the test cylinder and its cylindrical supports was calculated using the above equation. It was found that the maximum total blockage correction would amount to free stream velocity changes of approximately one percent. That is, the local free stream velocity, U_F, was:

$$U_F = 1.01\ U \qquad (15)$$

Even though this correction is very small, it was applied to all the free-stream velocity measurements.

3.3.2 Free-Stream Turbulence Effects

Some of the discrepancies observed among previous experimental results on heat transfer to cylinders can be attributed to the difference in free-stream turbulence intensities in the different investigations [7]. Increasing the intensity of free-stream turbulence will produce the following results [18]:

1. Earlier transition to turbulence in the boundary layer, and hence an increase in heat transfer rate which is characteristic of a

turbulent flow as compared with a laminar boundary layer.

2. Increase of heat transfer in the laminar portion of the boundary layer. At large turbulence intensities, a system of stationary, counter rotating vortices are set up in the boundary layer of the cylinder. Those vortices are the result of non-linear amplification of Taylor-Görtler instability modes in the transition process and produce a highly three-dimensional flow over the cylinder. The three-dimensional boundary layer flow increases the heat transfer rate.

Kaylar [19] has investigated the effect of turbulence intensity on the transfer of heat from a circular cylinder. He has found that turbulence intensities below 1% have negligible effect on the heat transfer rate, as shown in Figure 11. The free-stream turbulence intensity of the wind tunnel in which this investigation was conducted was well below 1% as seen in Figure 2. It has been estimated that Hilpert's experimental data, on which Morgan's correlations are based, were obtained at free-stream turbulence intensity levels of 0.9% [20]. Therefore, it was concluded that the difference in the free stream turbulence intensity of this experimental investigation and that of Hilpert's would not cause significant discrepancies in the heat transfer coefficients.

3.3.3 Natural Convection Effects

At high Reynolds numbers, heat transfer occurs mainly by the process of forced convection, but as the Reynolds number decreases, the contribution due to natural convection becomes significant. It was decided to investigate whether natural convection had a significant contribution to the heat transfer process at the lowest Reynolds number used in this experiment

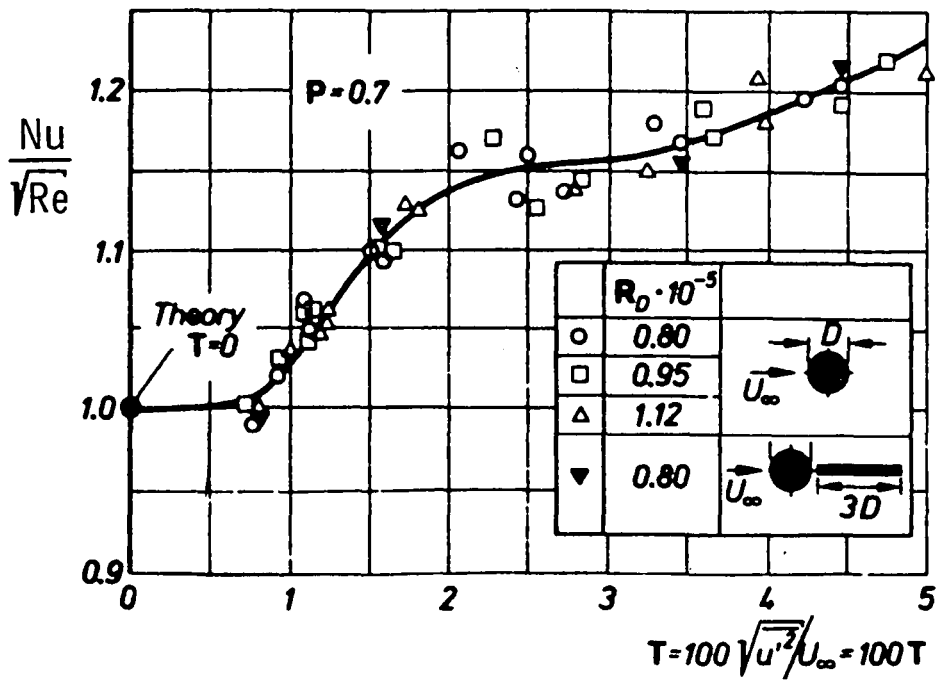

Fig. 11. Effect of free stream turbulence intensity on the rate of heat transfer in the stagnation region of a cylinder, after L. Kaylar [19].

(1800). The nominal temperature difference between test cylinder's surface and free stream was about 15°C at this condition. This temperature gradient would yield a Nusselt number based on pure natural convection of about 3. The corresponding pure forced convection Nusselt number would be approximately 20.

Much confusion has existed over calculating the Nusselt number when both natural and forced modes of convection are present. Morgan [7] has recommended using an effective Reynolds number for calculating total heat transfer by Equation 1. This effective Reynolds number is given by:

$$Re_{eff} = \sqrt{(Re^* + Re \cos \xi)^2 + (Re \sin \xi)^2} \qquad (16)$$

where:

ξ = angle between direction of flow and the vertical direction of natural convection flow

Re^* = equivalent Reynolds number for natural convection

The equivalent Reynolds number is found by equating the Nusselt number for natural and forced flows. For natural flows, the Nusselt number is calculated [7] by:

$$Nu = B_1 (Gr \cdot Pr)^{m_1} \qquad (17)$$

where:

Gr = Grashof number

Pr = Prandtl number

B_1, m_1 = constants depending upon the magnitude of GrPr

This yields:

$$Re^* = \left\{ \frac{B_1}{D_2} \; Pr^{m_1} \right\}^{1/n_1} \; Gr^{m_1/n_1} \qquad (18)$$

For the case of lowest flow speeds, Re = 1800, the equivalent Reynolds number is 26, having no significant effect on the effective Reynolds number. Thus, it was concluded that the effect of natural convection is negligible throughout the experiments.

3.4 Error Analysis

Measurement of any physical quantity involves some degree of error. The measured quantity is always disturbed by the act of measurement, which makes a perfect measurement practically impossible. Furthermore, all the measuring sensors used for typical experimental investigations have some degree of imprecision compared to the standard sensors -- the most accurate sensors employed by national laboratories. One major concern in any experimental investigation is the estimation of the accuracy of the individual measurements. That is, the estimation of how close the measured values are to the "true" values. The imprecision of any measurement is estimated by using statistical analysis of the sensors calibration data, or manufacturer's accuracy statements, or rough estimates based on the experience of the investigator.

The overall accuracy of any physical quantity computed using a few independent measurements can be estimated using the root-sum-square method [21]. That is, if N is a function of n independent measurements, u_1, u_2, ..., u_n:

$$N = f(u_1, u_2, \ldots, u_n) \qquad (19)$$

where the independent measurements have imprecisions of $\pm\Delta u_1$, $\pm\Delta u_2$, ..., $\pm\Delta u_n$, respectively, then the overall accuracy of N is:

$$E = \sqrt{\left(\Delta u_1 \frac{\partial f}{\partial u_1}\right)^2 + \left(\Delta u_2 \frac{\partial f}{\partial u_2}\right)^2 + \ldots + \left(\Delta u_n \frac{\partial f}{\partial u_n}\right)^2} \qquad (20)$$

where $\frac{\partial f}{\partial u_i}$ represents partial differentiation.

The overall accuracy of the Reynolds numbers and Nusselt numbers obtained in this experimental investigation were estimated using the root-sum-square method. In order to accomplish this all the dependent variables used in the calculation of Nusselt number and Reynolds number had to be expressed in terms of the independent measured quantities. The expression for the Nusselt number was (using Equations 2 and 6):

$$Nu = \frac{V\ I}{\pi\ L\ k\ (\overline{T}_s - T_\infty)} \qquad (21a)$$

where the effect of radiation exchange has been neglected for simplicity of analysis. The expression for Reynolds number was (using Equations 8, 9, 10):

$$Re = \frac{D}{\mu\ T_m} \sqrt{\frac{2}{287}\ P_s\ P_d\ T_\infty} \qquad (21b)$$

The thermal conductivity and viscosity were not independent measurements,

and were calculated as a function of mean temperature, T_m. Therefore, they had to be expressed in terms of the independent measurements, T_s and T_∞. Dry air data for these thermophysical properties [13] were curve fitted for the temperature range of 283 to 313 K:

$$k = 3.92 \times 10^{-3} + 3.7 \times 10^{-5} \quad (T_s + T_\infty) \qquad w/mK \qquad (22a)$$

$$\mu = 4.39 \times 10^{-6} + 2.35 \times 10^{-8} \ (T_s + T_\infty) \qquad N.S/m^2 \qquad (22b)$$

The corresponding standard deviations of curve fitted data from the dry air tables were 1.68% and .01% for thermal conductivity and viscosity, respectively. These expressions were substituted in Equation 21a and 21b, and root-sum-square method was applied to the set of experimental data for the bare cylinders. The following imprecisions for the independent measurements were used:

Temperatures

Total temperature uncertainty was estimated at ± 0.25°C, due to sensor imprecision, ice point reference junction uncertainty, and temperature distortions caused by the sensor in the measuring medium.

Voltage and Current

Uncertainties in the voltage and current were assumed to be .8 mV and 4mA based on statistical analysis of experimental results.

Lengths

The length and diameter of the test cylinder were assumed to have uncertainties of 5 and .03 mm, respectively.

Pressures

The uncertainty in pressure measurements were estimated based on manufac-

turer's accuracy statements and analysis of experimental results.

Percent of Full Scale	Uncertainty
0 - 10%	1.2% of reading + 0.02% of full scale
10 - 100%	1.4% of reading + 0.02% of full scale

It was found that the maximum uncertainty in the Reynolds numbers and Nusselt numbers were 4.3% and 9.6%, respectively. The uncertainties at the different nominal Reynolds numbers are presented in Table 5.

Table 5. Estimated uncertainties in the measured values of Reynolds number and Nusselt number.

Reynolds number	% Error in Reynolds number	% Error in Nusselt number
14,000	2.8	9.6
9,000	2.8	8.4
6,000	2.8	7.8
4,000	3.0	7.4
2,700	3.4	7.2
1,800	4.3	7.0

4. PRESENTATION AND DISCUSSION OF RESULTS

In order to validate the experimental procedure, the convective heat transfer to the bare cylinder was measured in the wind tunnel facility over the Reynolds number range of 1000 to 20,000. The data were obtained using the specified constant heating rate of 1040 w/m^2 based on the outside surface of the test cylinder. Two sets of data were obtained in two "iden-

tical" wind tunnel facilities.* The measured Nusselt numbers as a function of Reynolds number are shown in Figure 12 along with the correlation curve developed by Morgan [7]. The data have a standard deviation of 6.1% relative to Morgan's correlation, thus validating the experimental procedure.

The maximum observed surface temperature variation (among the four thermocouples) for the bare cylinder tests was found to be 0.15°C. Later, it was found that for the shrouded cylinder tests, the maximum observed surface temperature variation was 0.3°C. These results validated the assumption that the surface temperature variation was not significant, thus, justifying utilization of only four thermocouples for surface temperature measurement.

The convective heat transfer to shrouded cylinders was measured over the Reynolds number range of 1000 to 20,000 for three different sets of shrouds with radius ratios of 1.1, 1.4, and 2.1. Each set consisted of three shrouds with nominal ventilation factors of 0.09, 0.18, and 0.27, while the set of shrouds with a radius ratio of 1.1 had an additional shroud with a ventilation factor of 0.36. Each shroud was tested with two shroud orientations with respect to flow ($\theta = 0°$, $\theta = 30°$) as specified in Table 4. The set of shrouds with a radius ratio of 1.1 were also tested with shroud orientation of $\theta = 15°$. The results showing the variation of measured Nusselt numbers with Reynolds number and shroud orientation for each of the shrouds are shown in Figures 13 through 16. The correlation curve of Morgan [7] for convective heat transfer to bare cylinders is also shown in each figure. It should be noted that the Reynolds numbers were based on the bare cylinders diameter.

*The wind tunnel was disassembled and moved to another building during the course of this investigation.

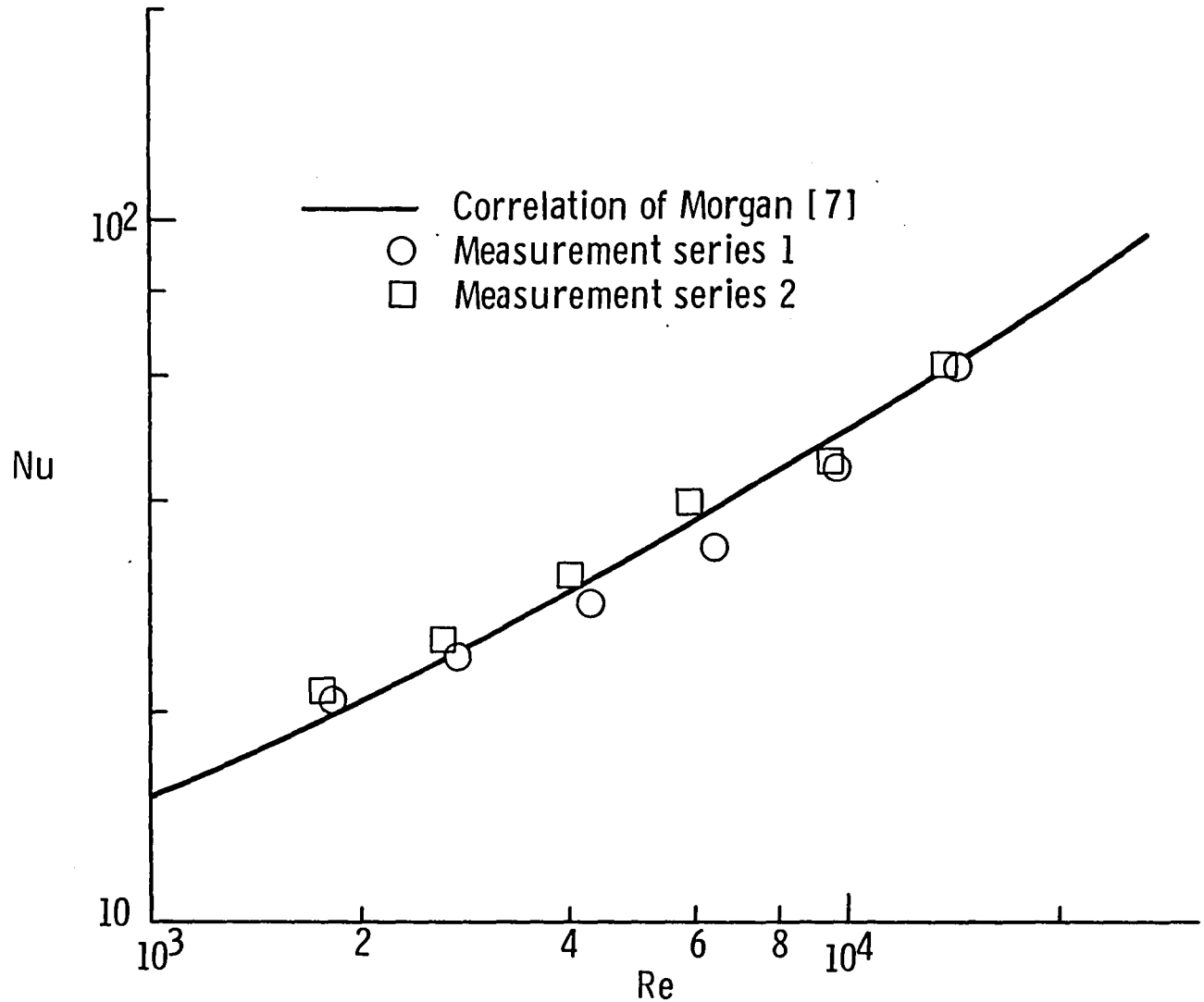

Fig. 12. Heat transfer data for bare cylinder.

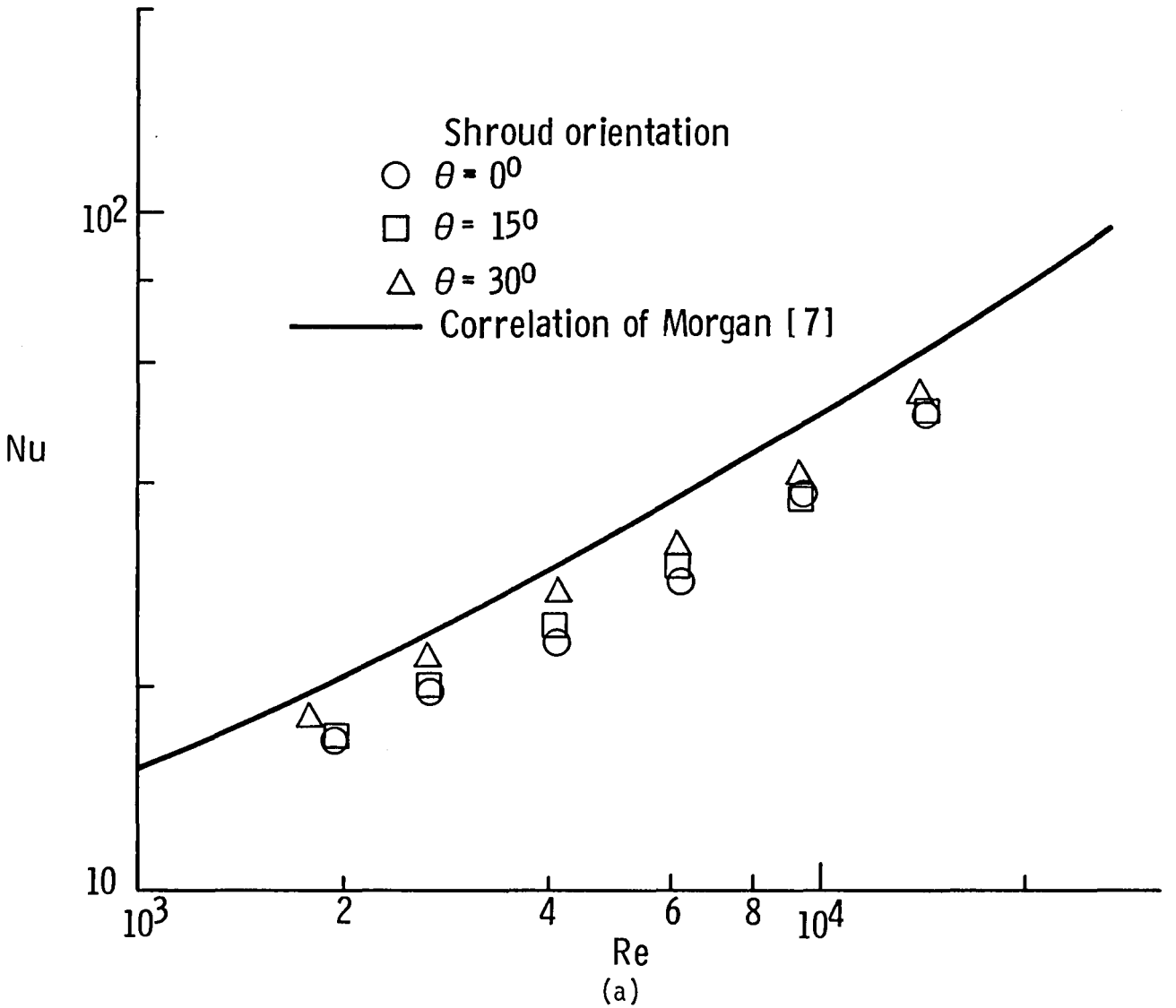

Fig. 13. Heat transfer data for perforated shrouds with ventilation factor of 0.09. a) ϕ = 1.1, b) ϕ = 1.4, c) ϕ = 2.1, and d) combination of three cases.

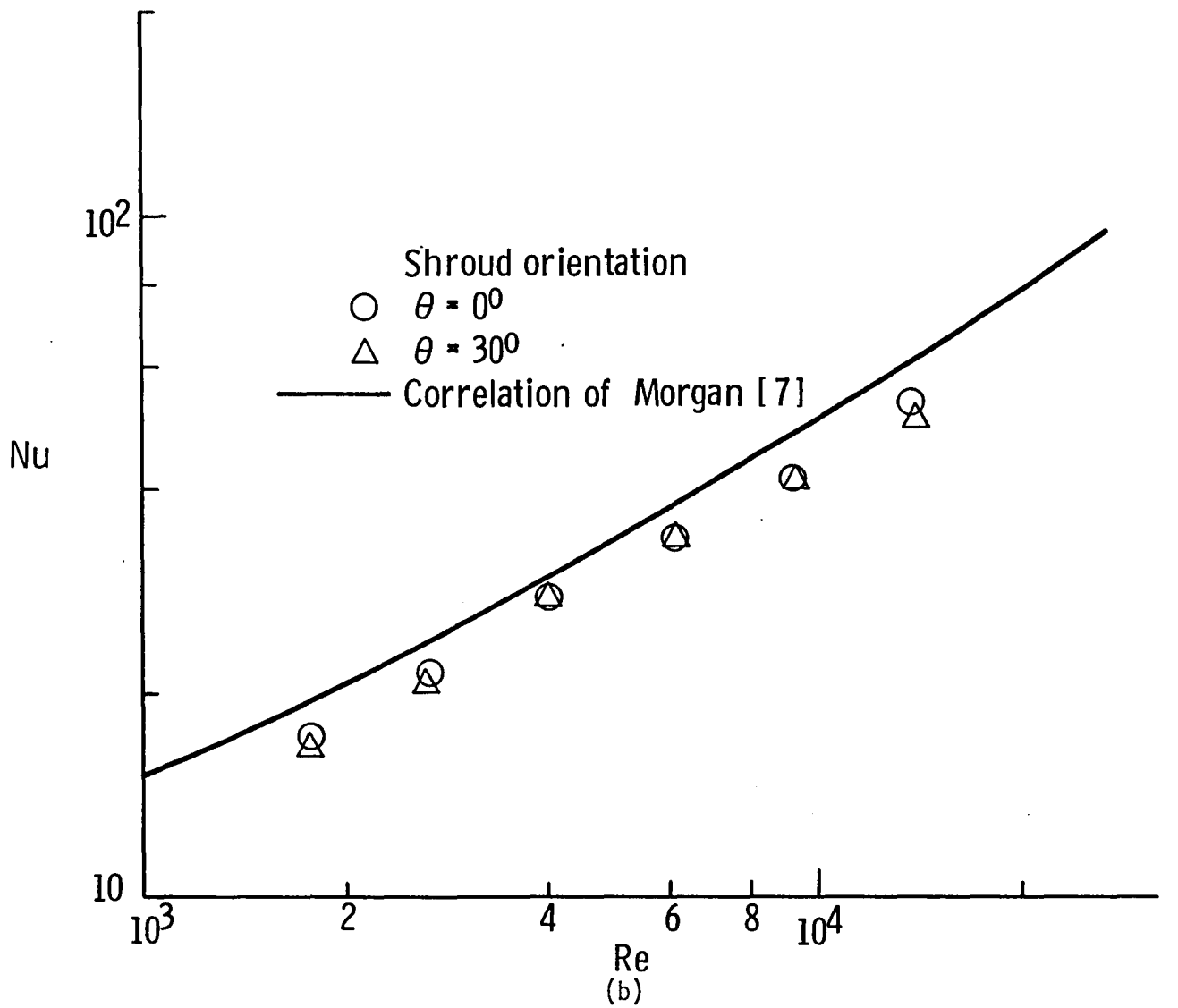

Fig. 13. (Continued).

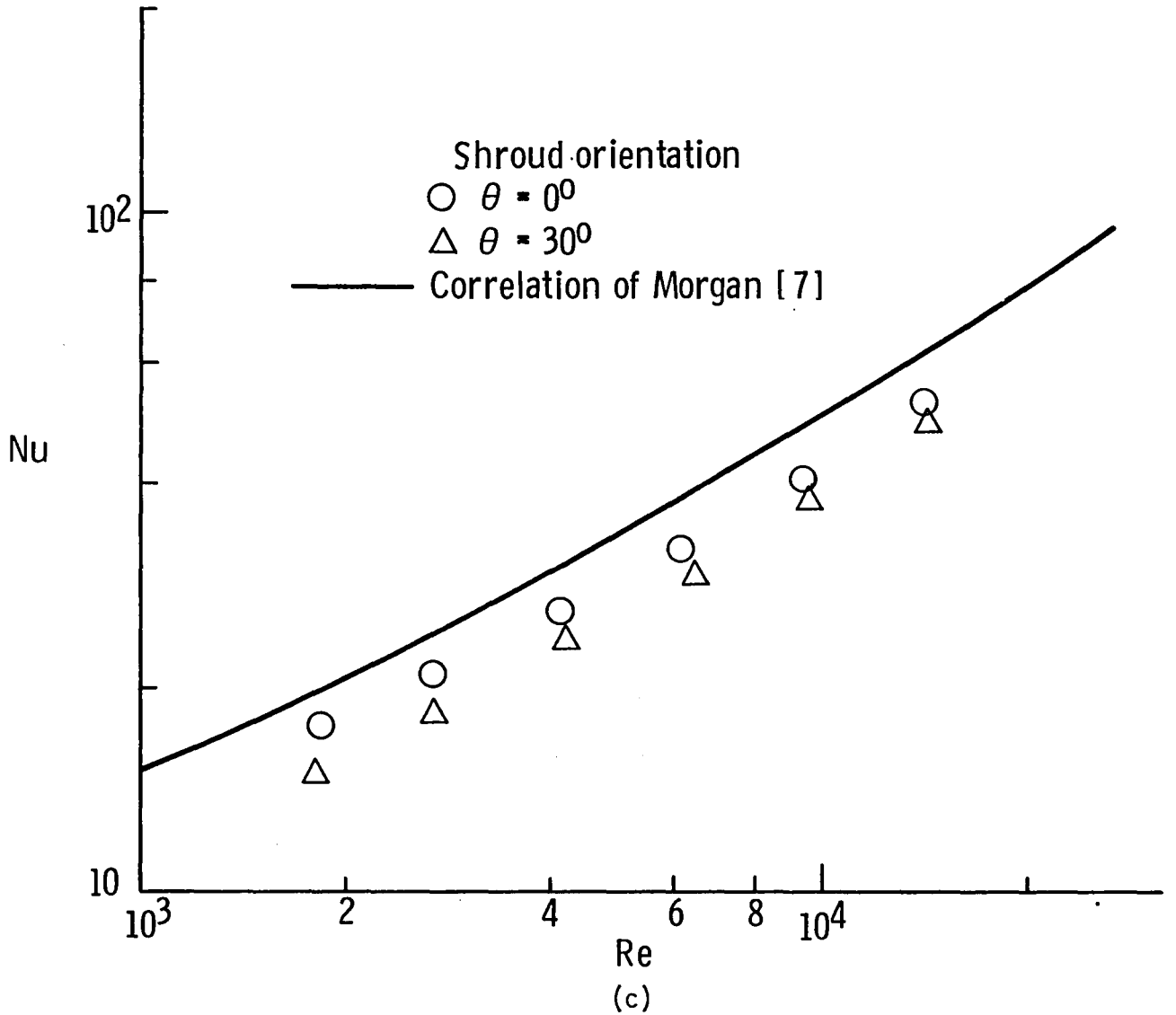

Fig. 13. (Continued).

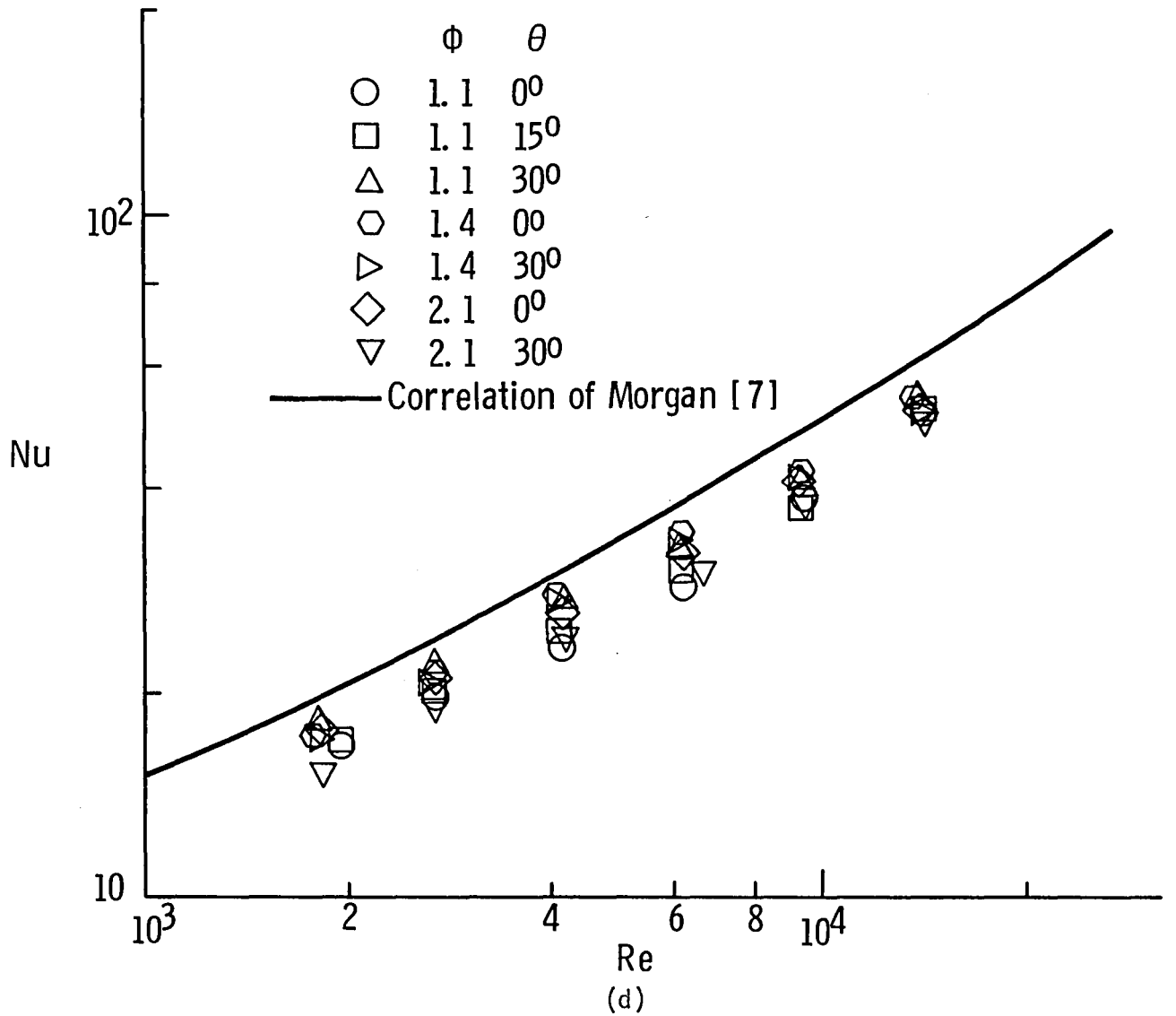

Fig. 13. (Concluded).

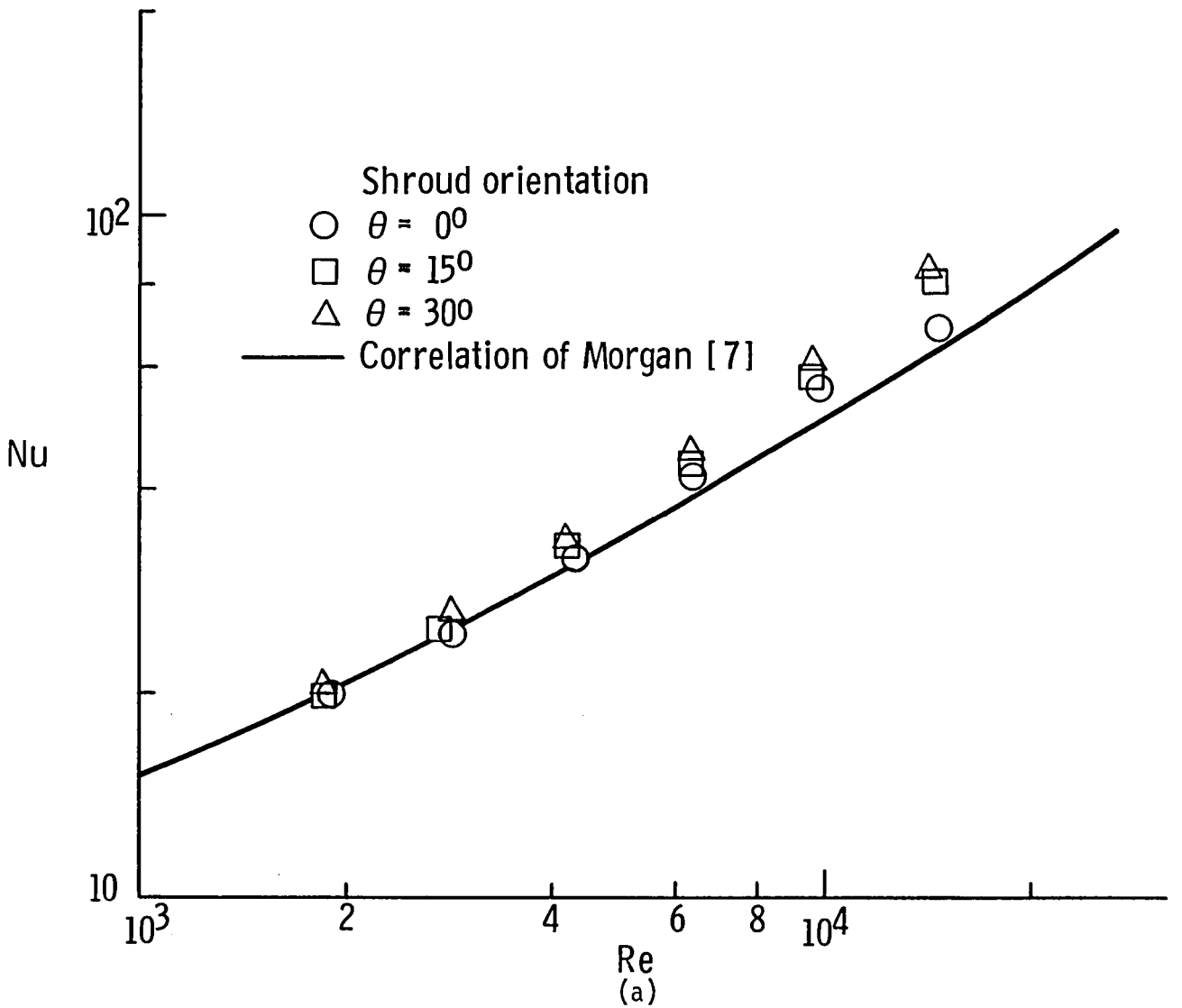

Fig. 14. Heat transfer data for perforated shrouds with ventilation factor of 0.18. a) ϕ = 1.1, b) ϕ = 1.4, c) ϕ = 2.1, and d) combination of three cases.

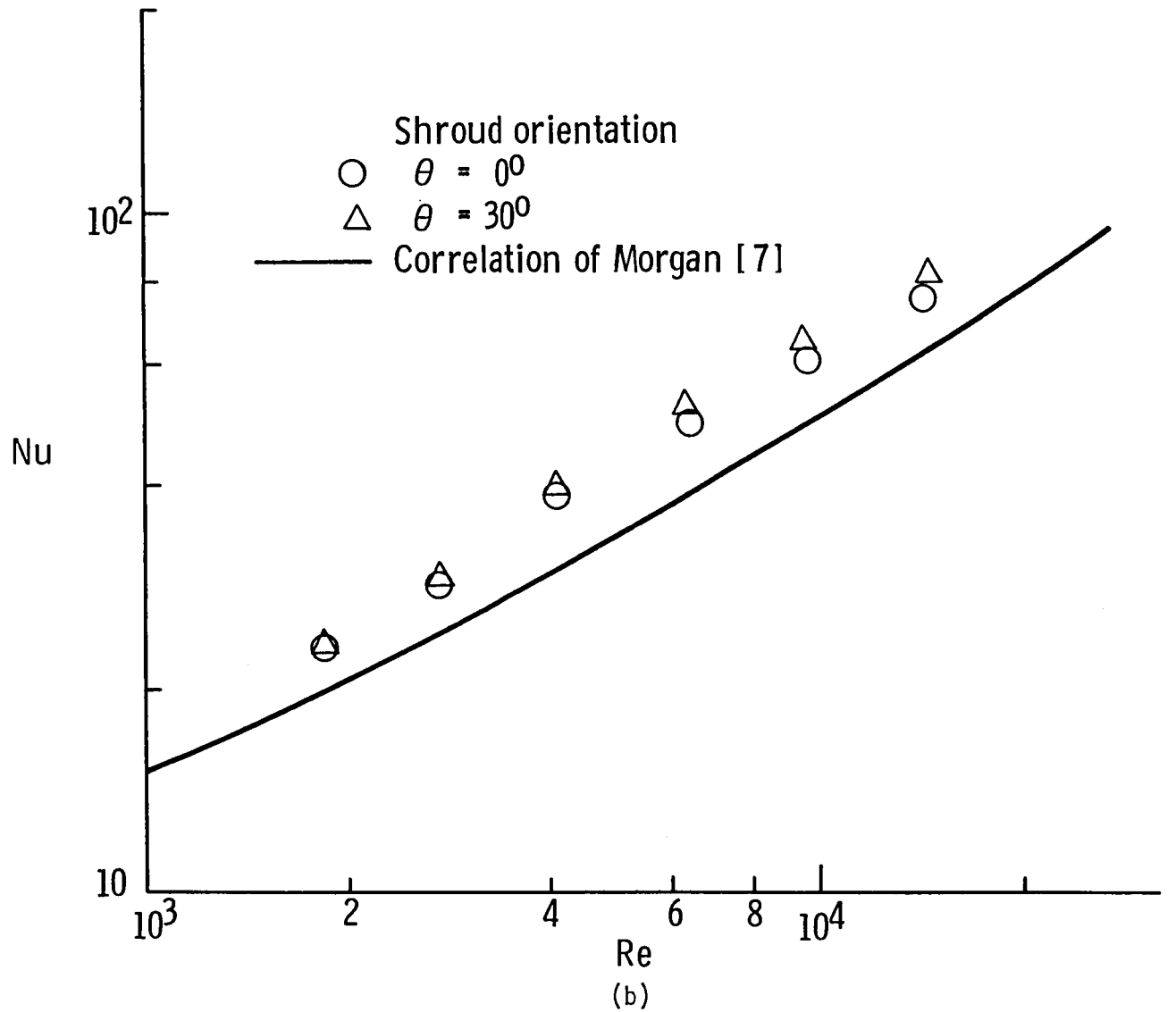

Fig. 14. (Continued).

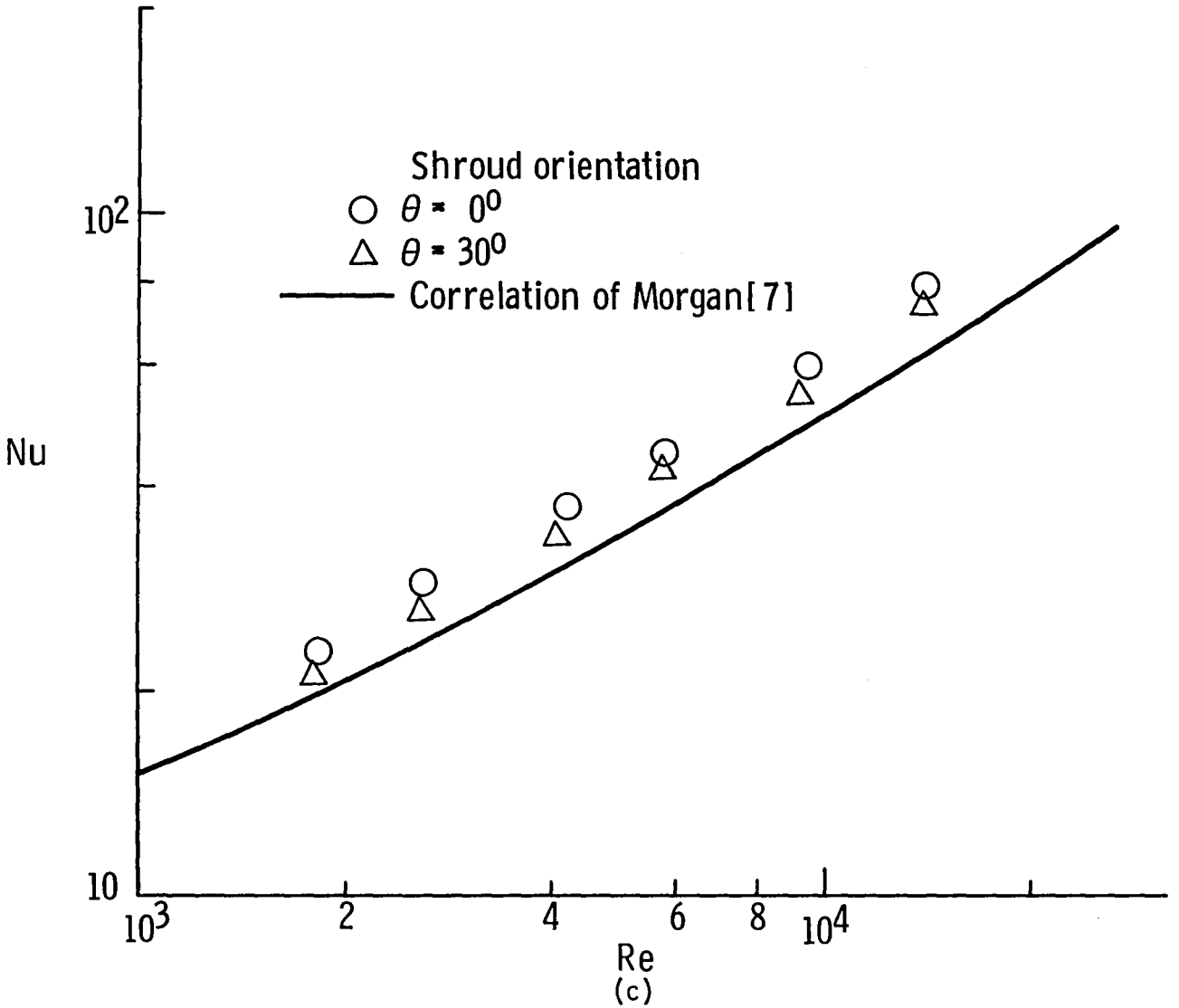

Fig. 14. (Continued).

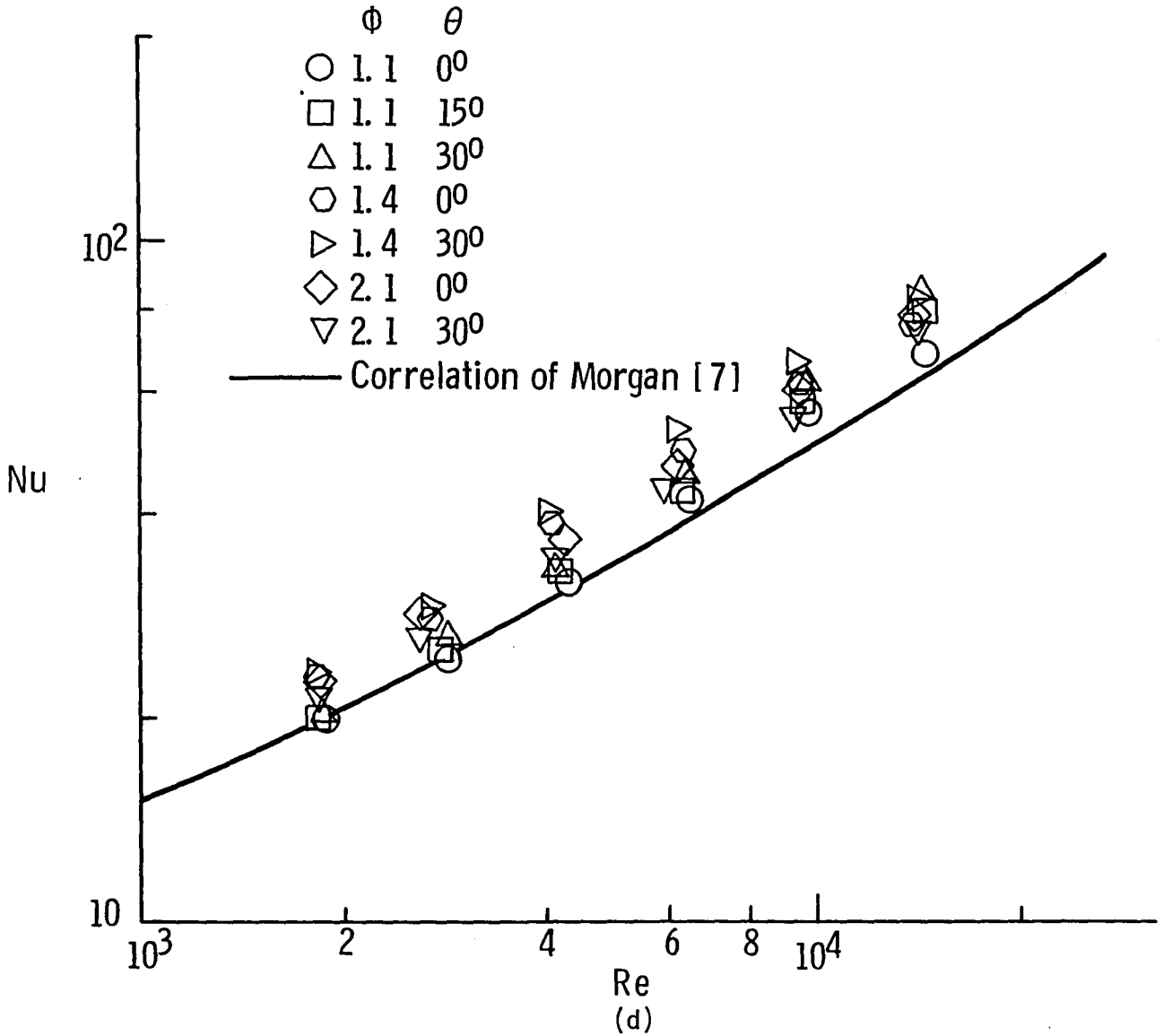

Fig. 14. (Concluded).

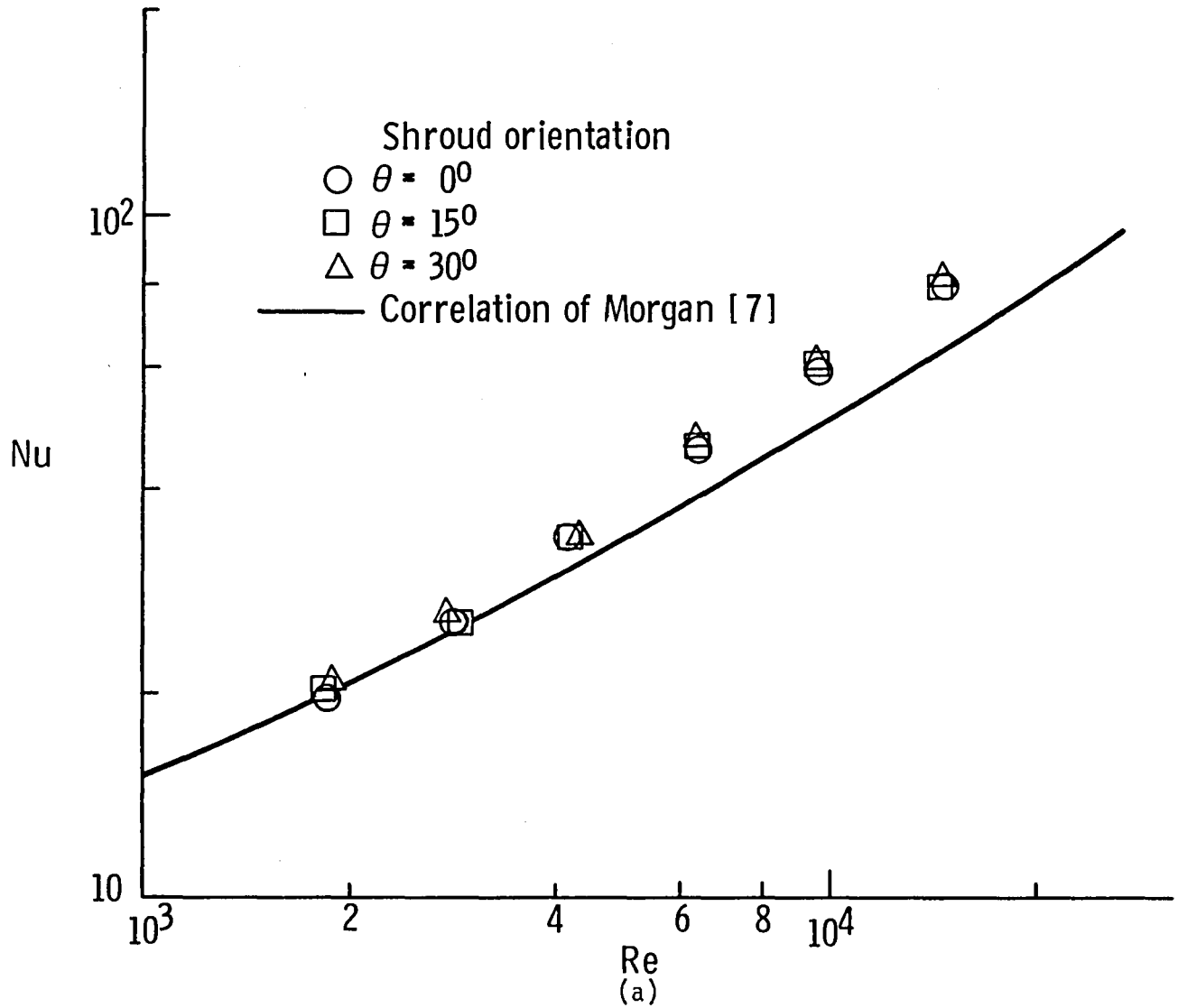

Fig. 15. Heat transfer data for perforated shrouds with ventilation factor of 0.27. a) ϕ = 1.1, b) ϕ = 1.4, c) ϕ = 2.1, and d) combination of three cases.

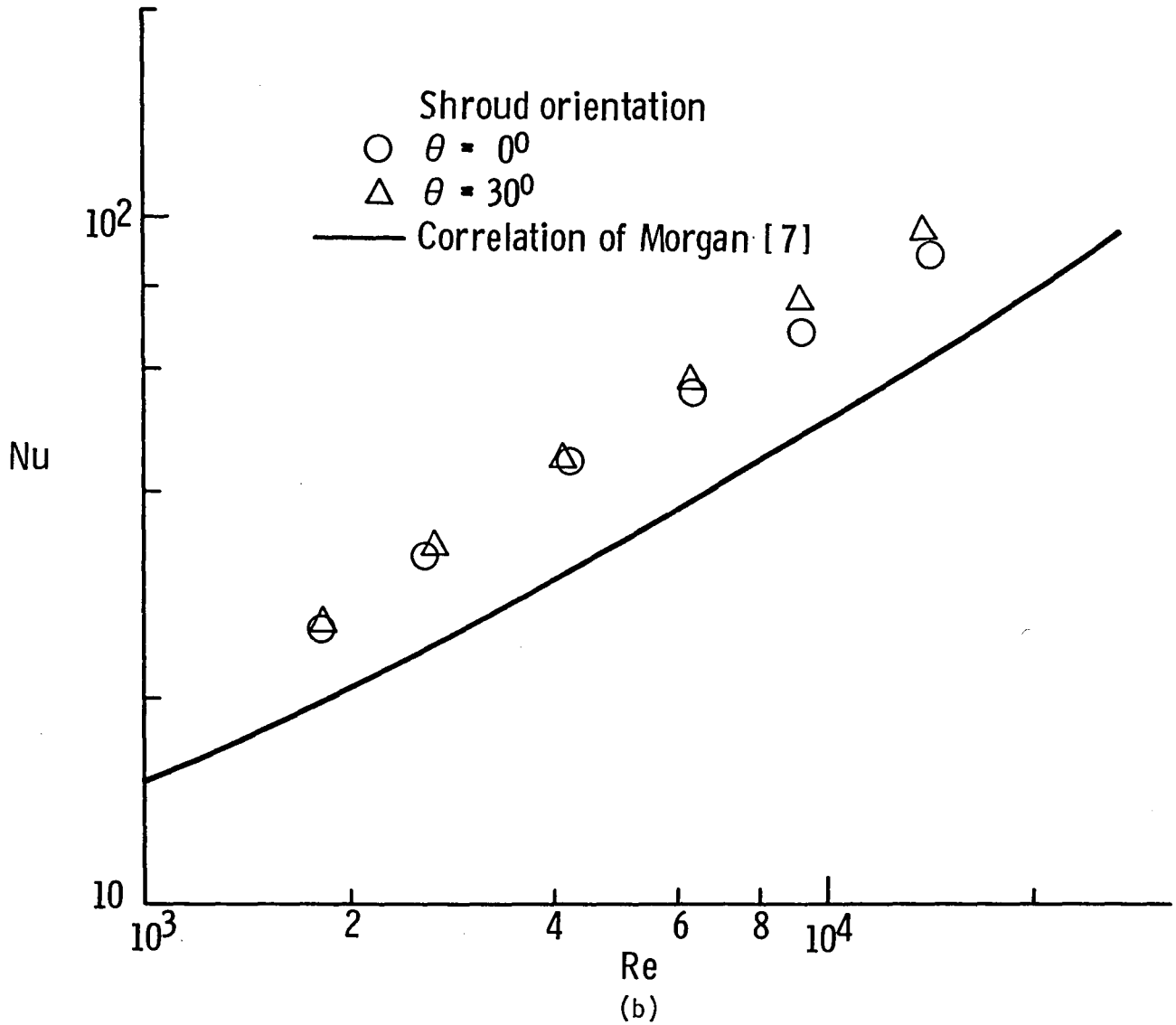

Fig. 15. (Continued).

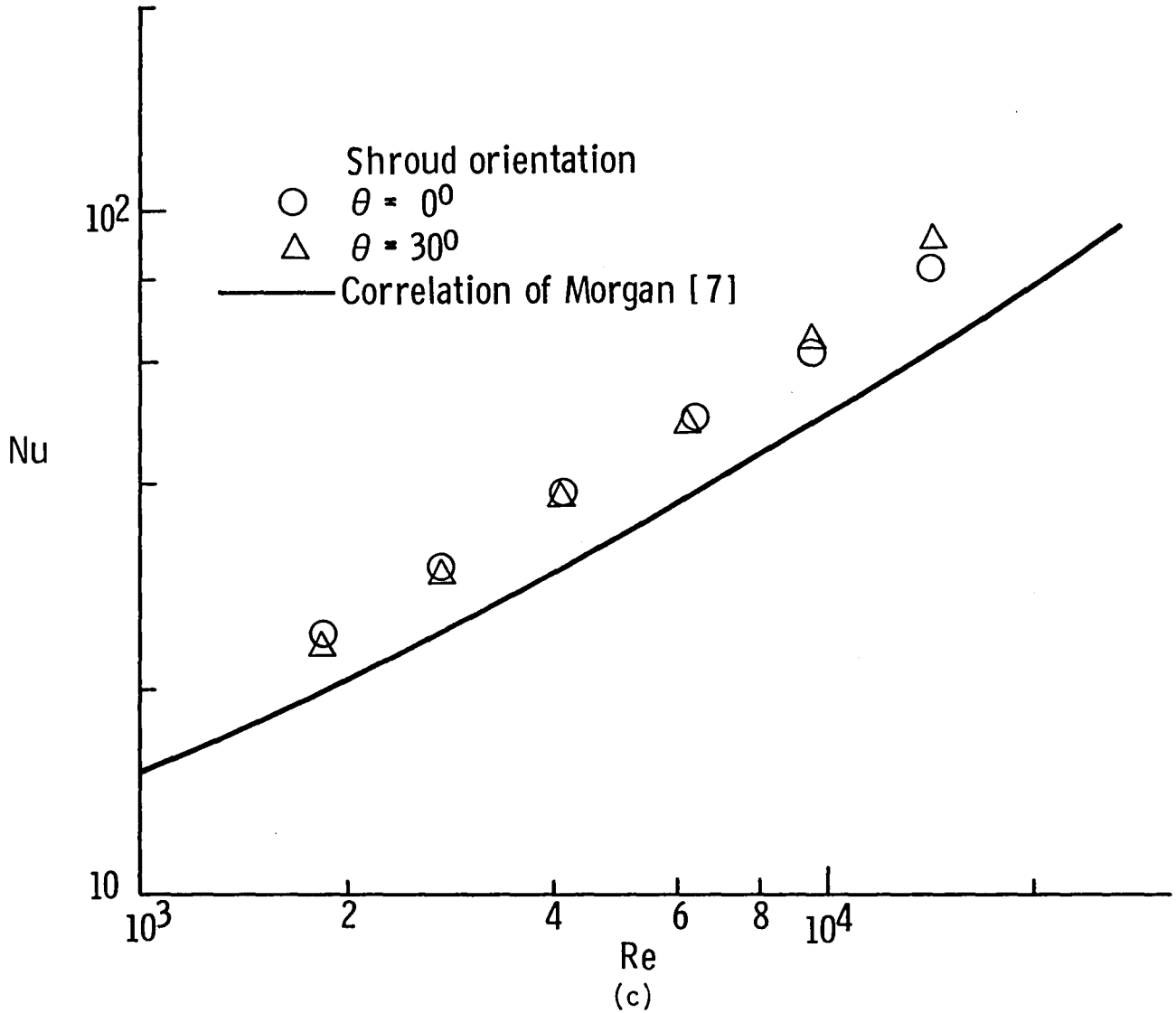

Fig. 15. (Continued).

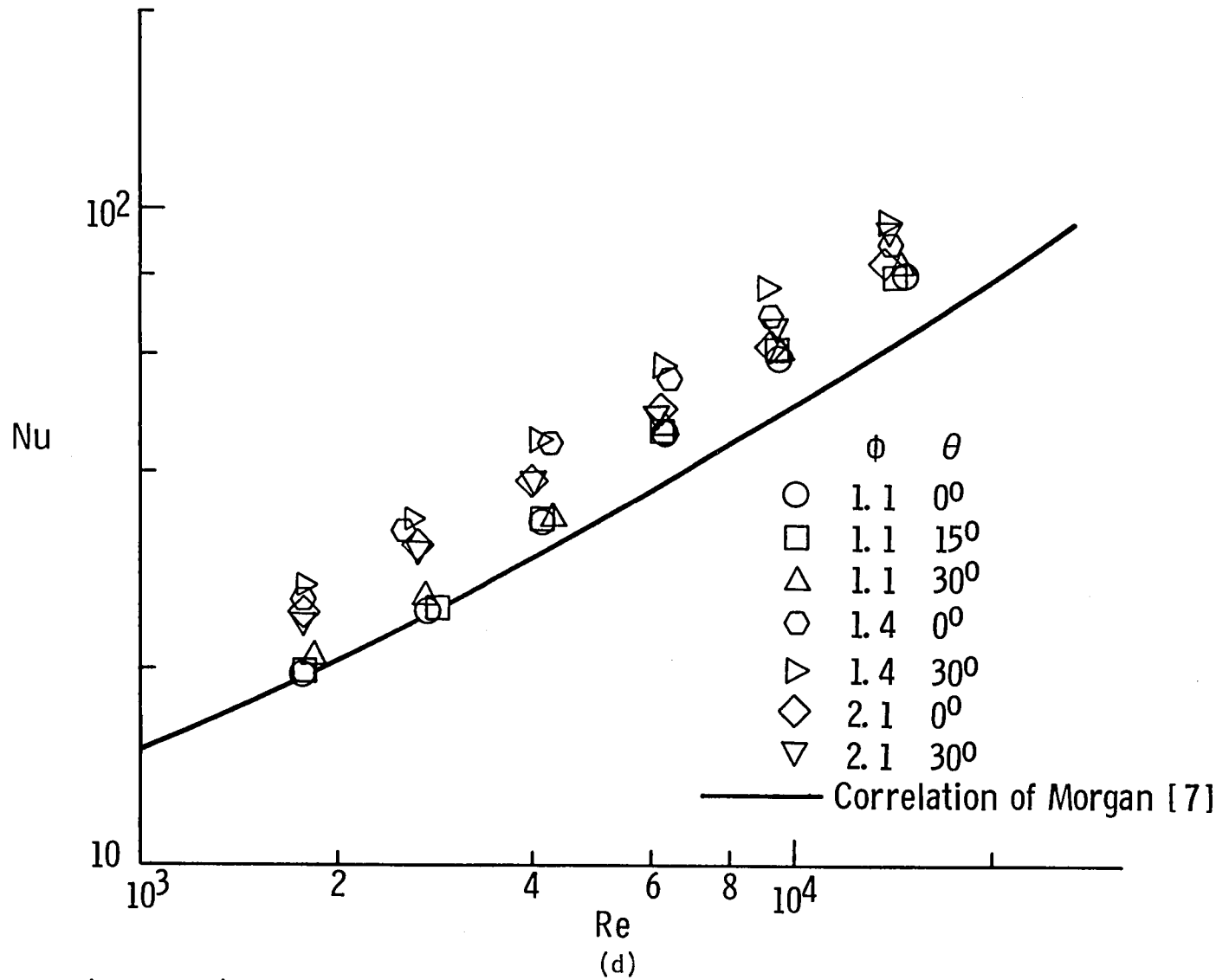

Fig. 15. (Concluded).

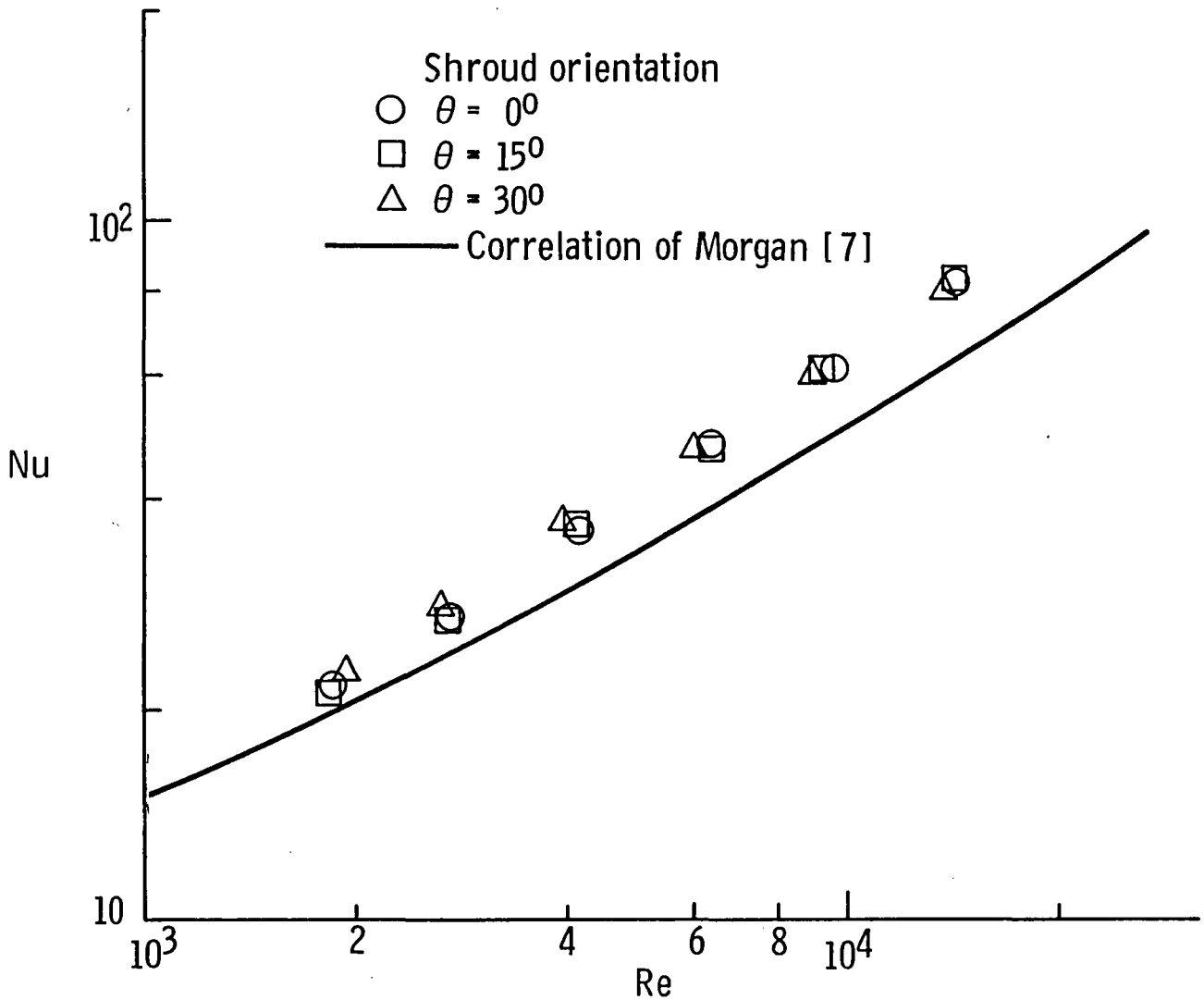

Fig. 16. Heat transfer data for perforated shrouds with ventilation factor of 0.36 (ϕ = 1.1).

The data indicate clearly that it is possible to enhance heat transfer to a solid cylinder by employing perforated shrouds (over the tested Reynolds number range). Convective heat transfer to the cylinder was enhanced as high as 50% for the shrouded case compared to bare cylinder in some cases. It can be seen that shrouds with ventilation factor of .09 retarded the convective heat transfer to the cylinder, while shrouds with ventilation factors of .18 and higher clearly enhanced the heat exchange. Shroud orientation influences the heat transfer with maximum heat transfer generally occurring when the holes are centered on either side of the stagnation line ($\theta = 30°$), but that effect is of the second order compared to the ventilation factor and radius ratio.

In order to interpret the ventilation factor more clearly, curves were fared through the experimental data for the shrouds with a radius ratio of 1.1 for each shroud orientation over the Reynolds number range tested, recognizing the fact that the shroud ventilation factor has no effect at Reynolds numbers approaching zero. Then, the fared curves were used to estimate a "smoothed" Nusselt number for each ventilation factor and shroud orientation at selected Reynolds numbers between 1800 and 14000. Then the estimated Nusselt numbers were plotted against ventilation factor for different Reynolds numbers, as shown in Figure 17a. In order to generate the curves shown in this figure two assumptions were made. First, it was assumed that Nusselt number should equal the bare cylinder Nusselt number at a ventilation factor of unity. Second, it was assumed that for a ventilation factor of zero, the heat transfer is purely conductive between the shourd and the cylinder thus yielding a Nusselt number near unity. The Nusselt number represents the combined effects of heat conduction through the annulus and solid cylinder convection from the outside of the shroud.

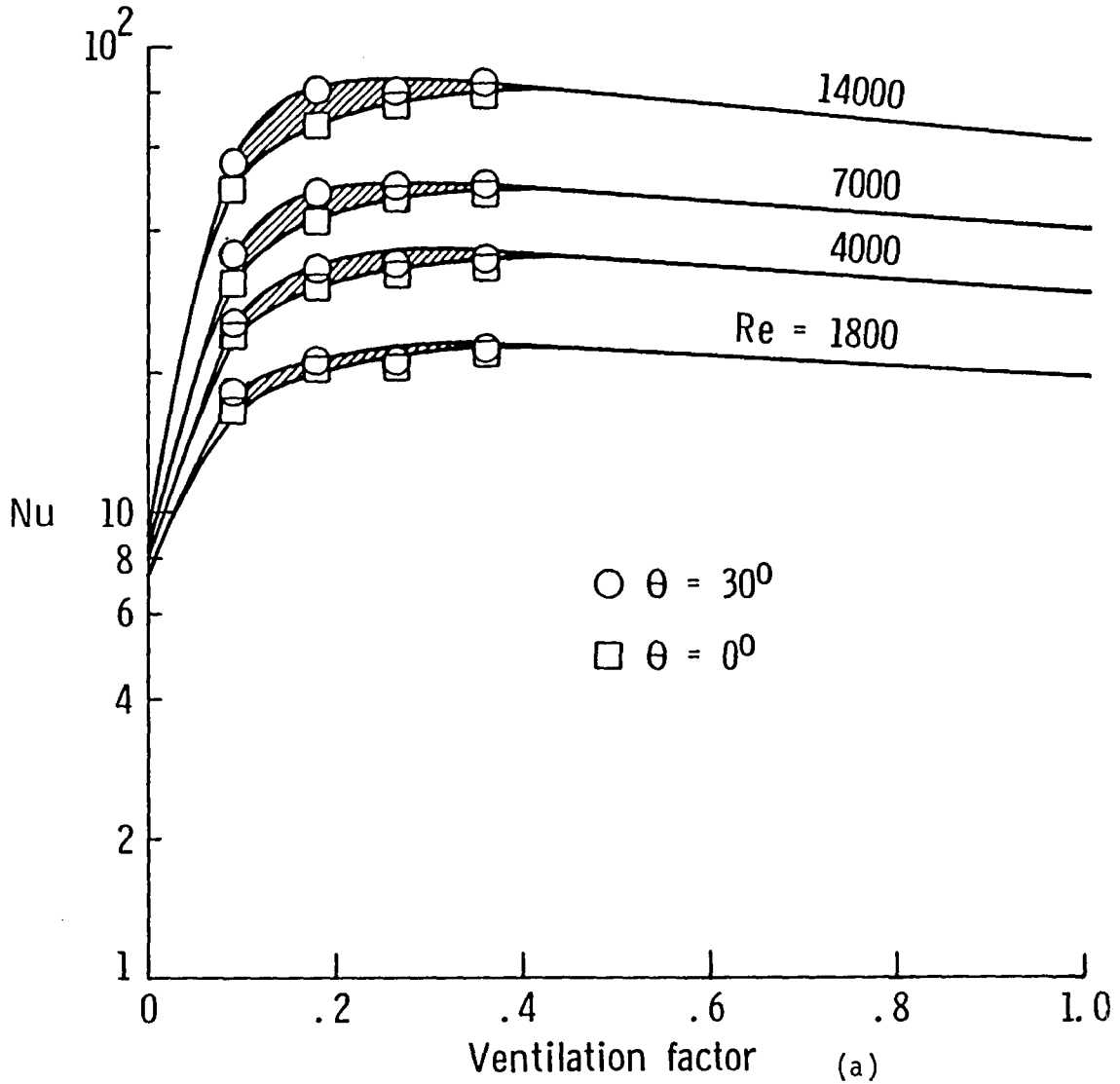

Fig. 17. Variation of extrapolated Nusselt number with ventilation factor for different Reynolds numbers. a) ϕ = 1.1, b) ϕ = 1.4, and c) ϕ = 2.1.

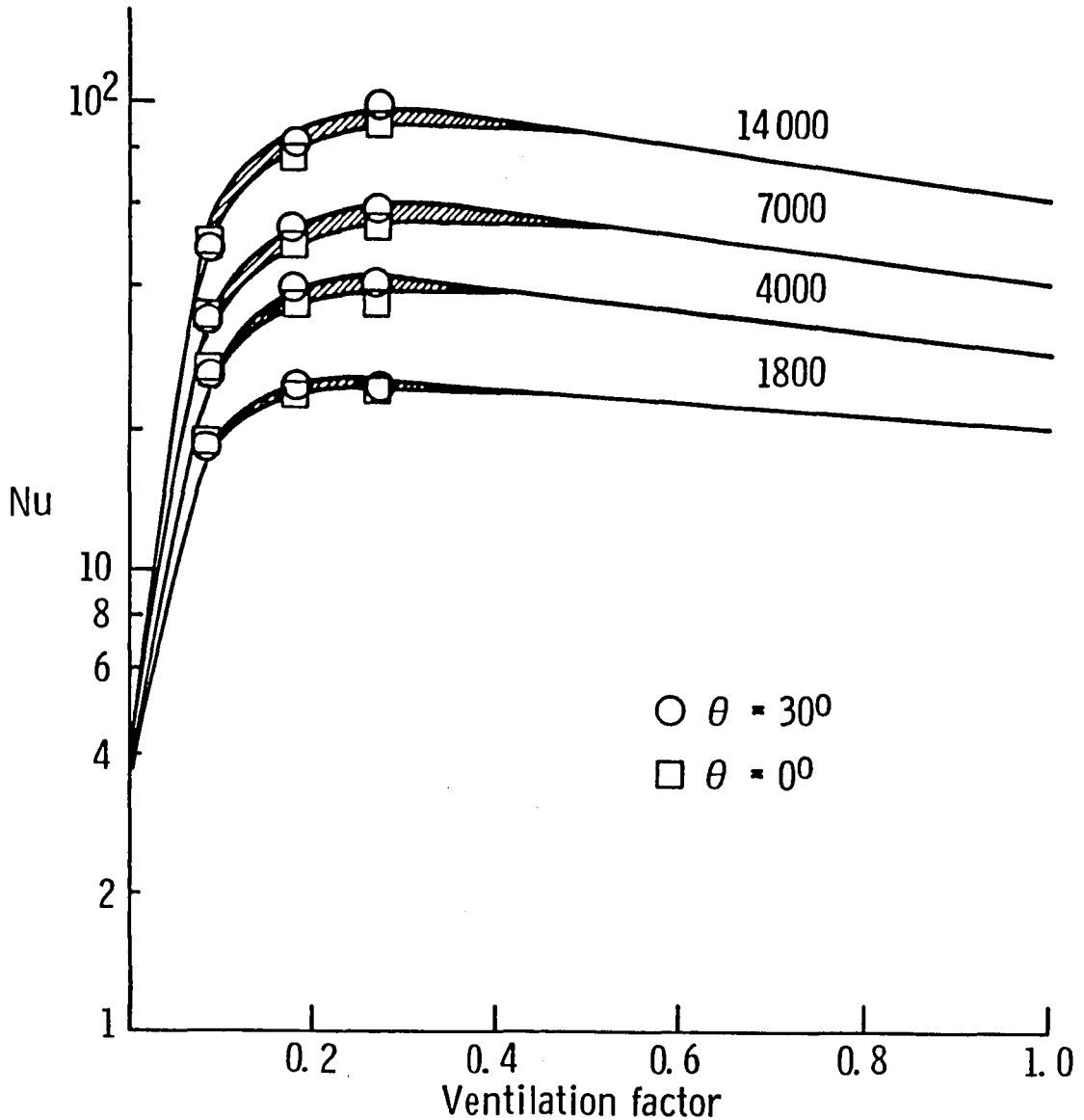

(b)

Fig. 17. (Continued).

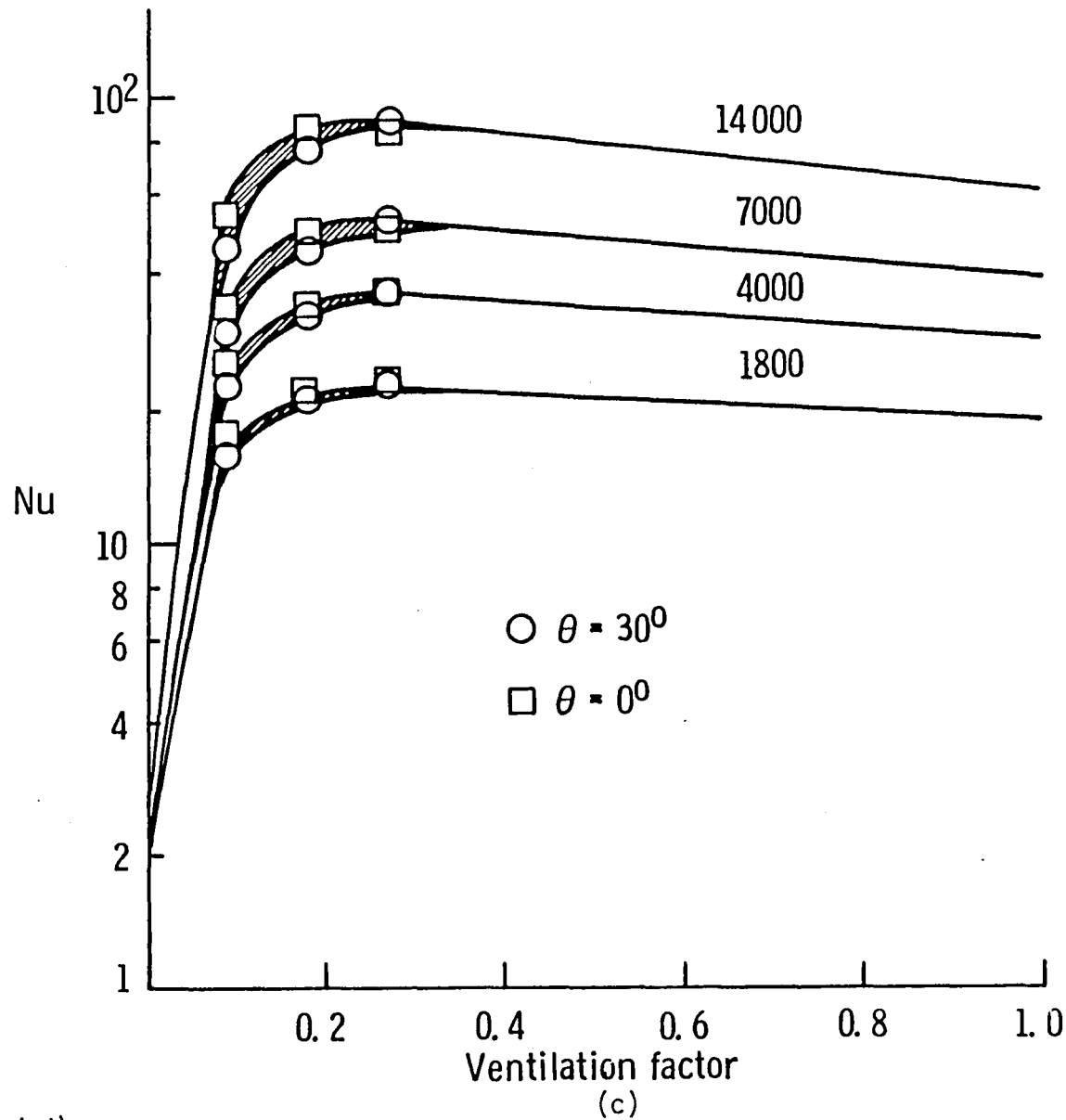

Fig. 17. (Concluded).

The shaded areas in Figure 17a represent the influence of shroud orientation. From this figure it can be seen that for ventilation factors near 0.2, the influence of the shroud on the convective heat transfer to the cylinder is favorable. Somewhat higher heat transfer occurs with the shroud in place than for the bare sensor at higher Reynolds numbers, but enhancement decreases as the Reynolds number decreases. For ventilation factors greater than approximately 0.2 the shroud becomes less effective. Furthermore, for ventilation factors less than 0.1, the shroud retards convective heat transfer to the cylinder. The same type of behavior was generally observed for the shrouds with radius ratios of 1.4 and 2.1 as shown in Figures 17b and 17c.

In order to study the combined effect of ventilation factor and radius ratio, it was decided to calculate an effective diameter, defined as the diameter which would yield a Nusselt number based on Morgan's correlation [7] equal to the experimentally measured Nusselt number, for each of the shrouded test cases. The results are presented in Table 6 where the average effective diameter of each shroud for the different shroud orientations and Reynolds numbers are presented as a function of ventilation factor and radius ratio. It was found that the effective diameter is basically independent of Reynolds number and shroud orientation. A dimensionless effective diameter defined as the ratio of the effective diameter to bare cylinder diameter is also presented in Table 6. The standard deviation of Nusselt numbers calculated using the given effective diameters in the Morgan's correlation with respect to the experimentally measured Nusselt numbers are also provided. The data indicate that the effective diameter could yield accurate estimations of the convective heat transfer for the perforated shroud case (in the range of experimental variables used). This

Table 6. Compilation of effective diameters for shrouds.

Radius Ratio	Ventilation Factor	Effective Diameter (mm)	Dimensionless Effective Diameter	Standard deviation of Nusselt numbers calculated using the effective diameter in Morgan's correlation [7] with respect to experimental data. (Values are in percentages).
1.1	.09	5.68 ± .65	.72	5.65
1.1	.18	9.41 ± 1.38	1.20	7.63
1.1	.27	10.01 ± 1.31	1.27	7.08
1.1	.36	11.08 ± .94	1.40	4.37
1.4	.09	6.22 ± .46	.79	3.96
1.4	.18	11.88 ± 1.05	1.50	4.86
1.4	.27	14.75 ± 1.14	1.87	4.38
2.1	.09	5.51 ± .54	.70	5.62
2.1	.18	10.37 ± .78	1.31	3.95
2.1	.27	12.47 ± .90	1.58	3.82

implied that the convective heat transfer for each of the shrouded cases differs from the convective heat transfer from the bare cylinder by the ratio of an effective diameter to the bare cylinders diameter raised to the appropriate power specified in Morgan's correlations [7]. Therefore, if the Reynolds number in Morgan's correlations is based on the given effective diameter, the thermal behavior of the shrouded cylinders can be predicted accurately (for the range of parameters specified here).

The variation of the effective diameter with ventilation factor for different radius ratios is shown in Figure 18. Third order polynomial curves were fared through the experimental data for each radius ratio recognizing the fact that the dimensionless effective diameter should equal zero for a ventilation factor of zero, and unity for a ventilation factor of unity. It can be seen from Figure 18 that the relationship between effective diameter and ventilation factor for different radius ratios is consistent. The three third order polynomials were similar in shape and only varied from each other by constant factors. The data indicate that for ventilation factors between 0.2 and 0.4, the shrouds yield high effective diameters, thus enhancing convective heat transfer to the bare cylinder. For ventilation factors greater than 0.4, the shroud becomes less effective, while for ventilation factors less than 0.1, the shroud retards the convective heat transfer. It can also be seen that the greatest enhancement of heat transfer occurs with a radius ratio of 1.4. Increasing the radius ratio above this value makes the shroud less effective. Another observation is that for a radius ratio of 1.4 with ventilation factors ranging from 0.2 to 0.4, the convective heat transfer to the shrouded cylinder is higher than the convective heat transfer to a solid cylinder with a diameter equal to that of the shroud.

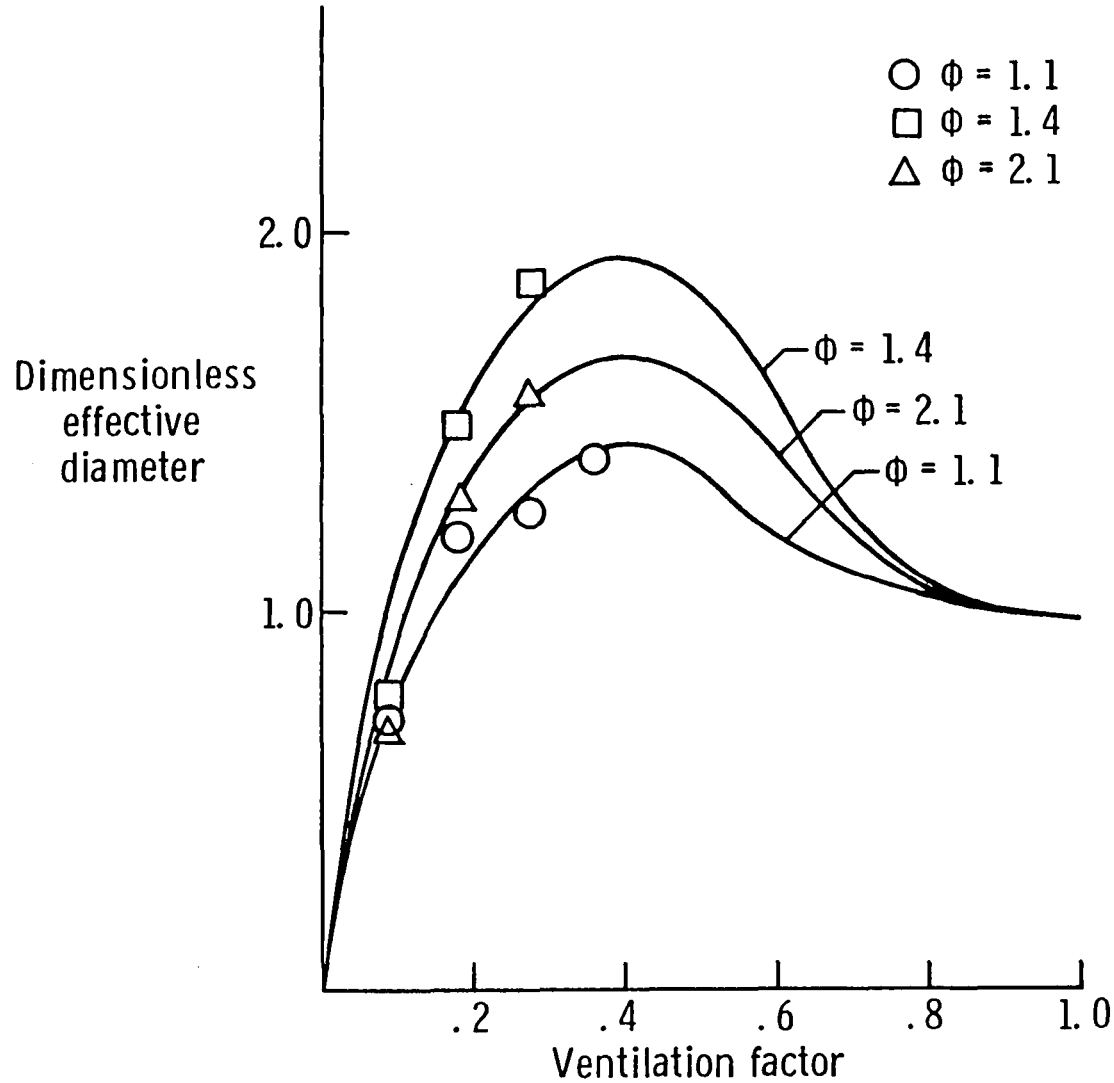

Fig. 18. Variation of effective diameter with ventilation factor for different radius ratios.

The variation of effective diameter with radius ratio for different ventilation factors is shown in Figure 19. Third order polynomial curves were fared through the experimental data for each radius ratio using the requirement that the dimensionless effective diameter should equal unity as radius ratio approaches infinity. This requirement was based on the assumption that as radius ratio tends to infinity the effect of shroud on the convective heat transfer becomes negligible, given an adequate ventilation factor. It can be seen that the convective heat transfer to the cylinder is enhanced by using a radius ratio of around 1.4.

Development of correlations between the effective diameter, ventilation factor, and radius ratio seemed inappropriate due to a limited number of data available. But the approximate variation of effective diameter with ventilation factor and radius ratio was obtained by incorporating the two-dimensional plots of Figures 18 and 19 into a three-dimensional plot as shown in Figure 20. It can be seen that the shroud enhances heat transfer to the bare cylinder for ventilation factors in the range 0.1 to 0.4 and radius ratio in the range 1.1 to 2.1. The maximum enhancement occurs for a radius ratio of 1.4 and ventilation factor between 0.2 and 0.3.

5. CONCLUSION

The influence of perforated cylindrical shrouds on the convective heat transfer to circular cylinders in transverse flow was measured experimentally. It was found that it is possible to estimate the convective heat transfer to a shrouded cylinder. The experiments showed that perforated shrouds with ventilation factors in the range 0.1 to 0.4 and radius ratios between 1.1 to 2.1 could enhance the convective heat transfer to bare cylinders considerably. This enhancement in some cases produced heat transfer coeffi-

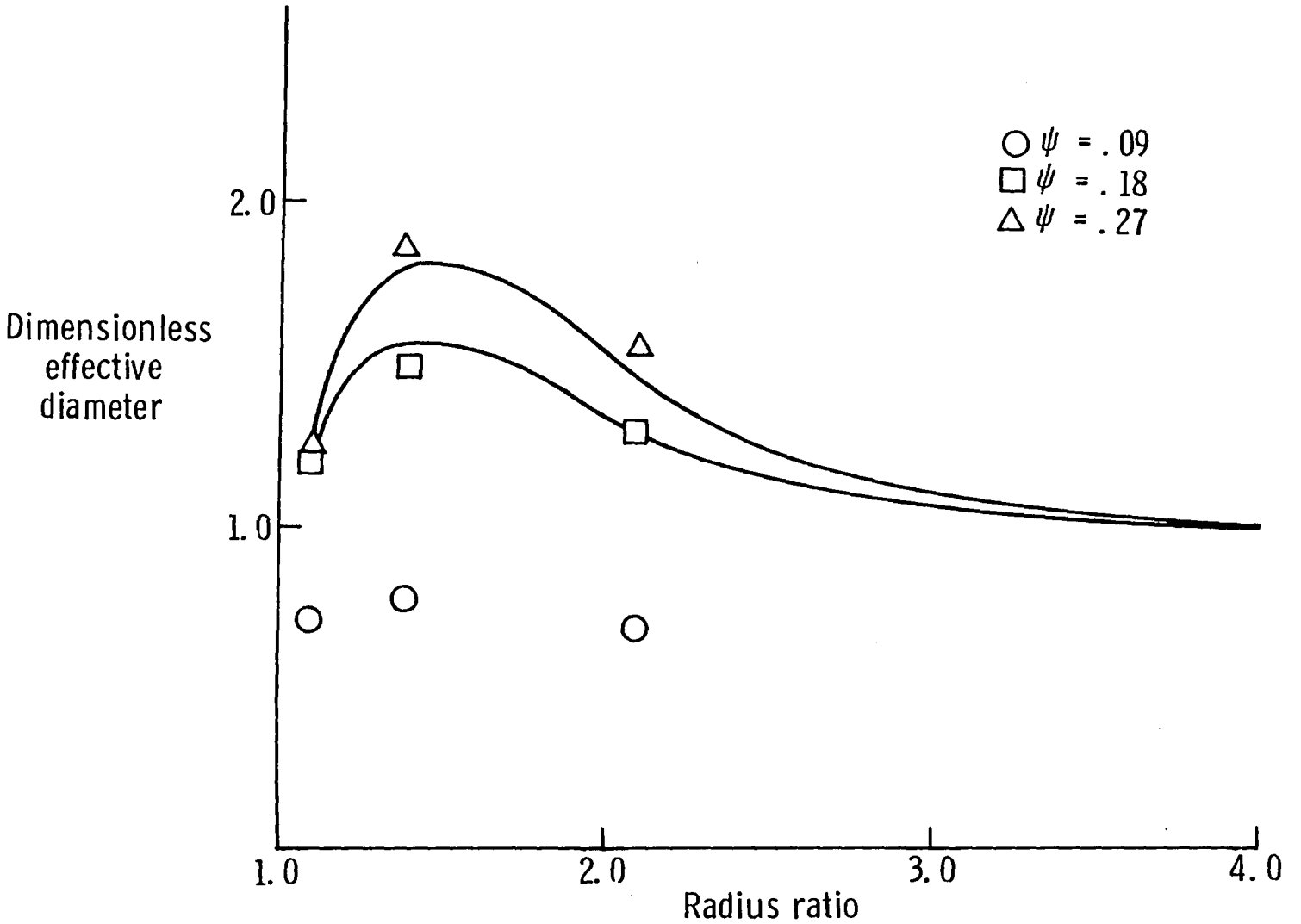

Fig. 19. Variation of effective diameter with radius ratio for different ventilation factors.

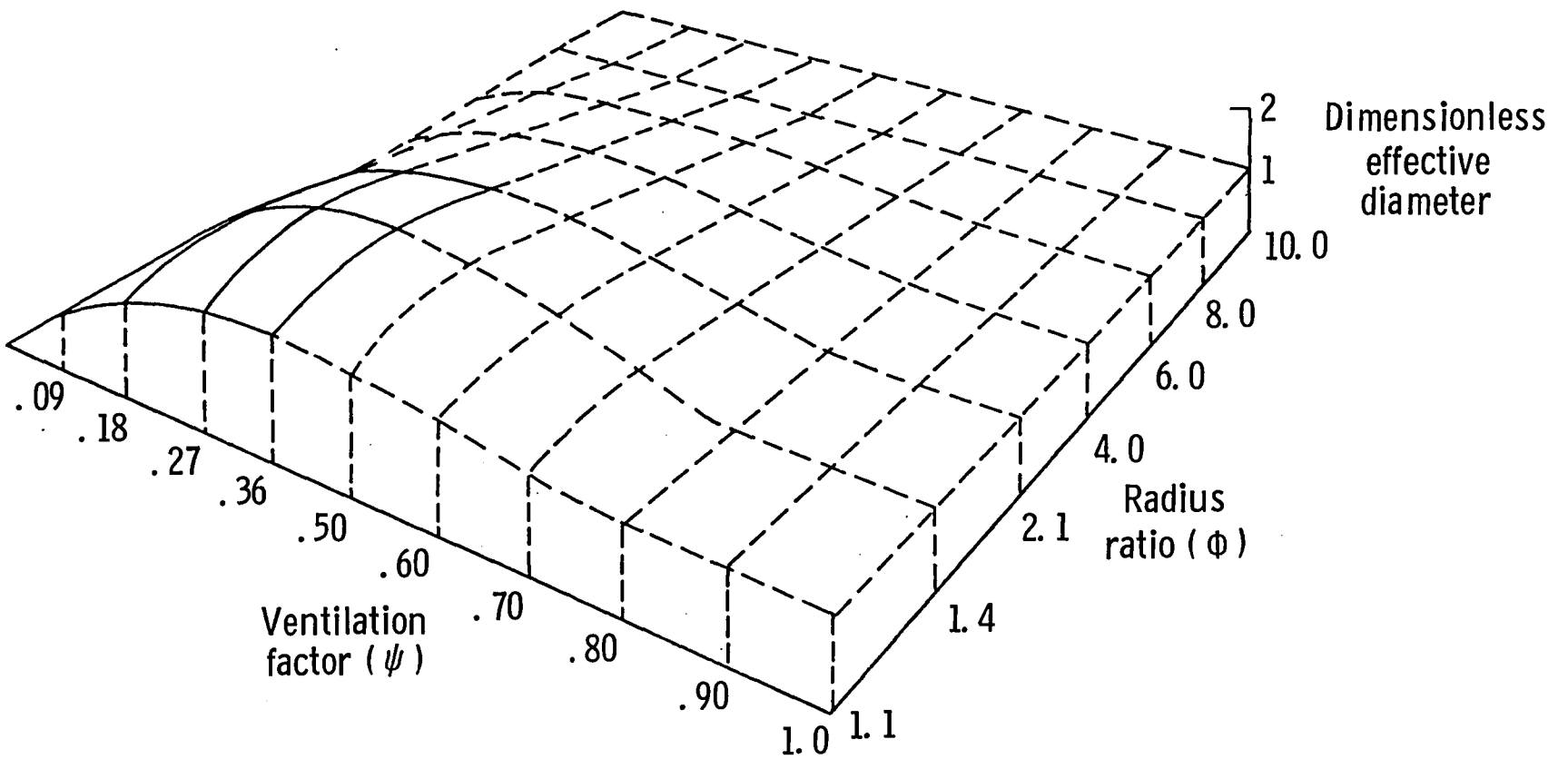

Fig. 20. Variation of effective diameter with ventilation factor and radius ratio.

cients that were higher than those achieved by a cylinder having a diameter equal to that of the shroud. The maximum enhancement occurred with a radius of 1.4 and ventilation factor in the range of 0.2 to 0.3.

The influence of radius ratio and ventilation factor appears to be systematic and predictable. It was found that the convective heat transfer for each of the shrouded cases differed from the convective heat transfer for the bare cylinder by the ratio of an effective diameter to the bare cylinder diameter raised to the appropriate power specified in Morgan's correlations [7]. It was found that the effective diameters were independent of Reynolds number and shroud orientation and depended primarily on ventilation factor.

Based on the limiting cases for the ventilation factor (0 and 1) and radius ratio (1 and infinity), it can be concluded that the experiments performed in this investigation were taken in the region where effective diameter changes the most. That is to say that the edges of the graph shown in Figure 20 can be drawn purely on the basis of physical logic. The dashed lines have been extrapolated based on that logic too. The fact that the surface described by the solid lines represents the dome of maximum influence, suggests that effective diameter estimations can be made in the dashed region.

Shroud orientation influences the heat transfer, but that affect is modest compared to the affects of ventilation factor and radius ratio. Effect of shroud orientation was more significant at higher Reynolds numbers and for ventilation factors between 0.1 and 0.3. The maximum heat transfer generally occurred when the shroud holes were centered on either side of the stagnation line.

REFERENCES

1. Pandey, D. K., Dillon-Townes, L. A., and Ash, R. L., "Response Time Correlations for Platinum Resistance Thermometers," ISA Transactions, Vol. 31, 1985, pp. 587-597.

2. "Mean Forces, Pressures, and Flow Field Velocities for Circular Cylindrical Structures: Single Cylinder with Two-Dimensional Flow," Engineering Science Data Unit Series, Item 80025, ESDU International Ltd., London, England, 1981.

3. Price, P., "Suppression of the Fluid-Induced Vibrations of Circular Cylinders," Journal of the Engineering Mechanics Division, Proceedings of ASCE, Vol. 82, 1956.

4. Walshe, D. E., (Appendices by Bearman, P. W.), "An Aerodynamic Investigation for the Proposed 850 Ft. High Chimney Stack for the Drax Power Station," National Physical Laboratory Aero Report 1227, 1967.

5. Warshawsky, I., "Heat Conduction Errors and Time Lag in Cryogenic Thermometer Installations," ISA Transactions, Vol. 13, 1974, pp. 335-346.

6. Daryabeigi, K., Ash, R. L., and Germain, E. F., "Measurement of Convective Heat Transfer to Solid Cylinders Inside Ventilated Shrouds," AIAA Paper 84-1725, presented at the AIAA 19th Thermophysics Conference, Snowmass, Co., 1984.

7. Morgan, V. T., "The Overall Convective Heat Transfer from Smooth Circular Cylinders," Advances in Heat Transfer, Vol. 11, 1975, pp. 199-263.

8. Hilpert, R., "Wärmeabgabe von geheizten Drähten und Rohren im Luftstrom," Forschung Ing.-Wes., Vol. 4, 1933, pp. 215-224.

9. Schmidt, E., and Wenner, K. (Transl. by J. Vanier), "Heat Transfer Over the Circumference of a Heated Cylinder in Transverse Flow," NACA TM-1050, 1943.

10. Giedt, W. H., "Investigation of Variation of Point Unit Heat Transfer Coefficient Around a Cylinder Normal to an Air Stream," Transactions of ASME, Vol. 71, 1949, pp. 375-381.

11. Moeller, C. E., Noland, M., and Rhodes, B. L., "NASA Contributions to Development of Special-Purpose Thermocouples," NASA SP-5050, 1968.

12. Kreith, F., and Black, W. Z., "Radiation," Ch. 6, Basic Heat Transfer, Harper & Row Publishers, New York, 1980.

13. Kays, W. M., and Crawford, M. E., Convective Heat and Mass Transfer, 2nd Ed., McGraw-Hill Book Co., New York, 1980.

14. Eckert, E. R. C., "Engineering Relations for Friction and Heat Transfer to Surfaces in High Velocity Flow," Journal of the Aeronautical

Sciences, Vol. 22, 1955, pp. 585-587.

15. Pankhurst, R. C., and Holder, D. W., "Tunnel Interference Effects," Ch. 8, Wind Tunnel Technique, Sir Isaac Pitman & Son Ltd., 1965.

16. Batchelor, G. K., "Interference on Wings, Bodies, and Airscrews in a Closed Tunnel of Octagonal Section," Australian Council for Aeronautics Report ACA5, 1944.

17. Thom, A., "Blockage Corrections in a Closed High-Speed Tunnel," British Aeronautical Research Committee R&M 2033, 1943.

18. Schlichting, H., Boundary Layer Theory, 7th Ed., McGraw-Hill Book Co., New York, 1979, pp. 313-315.

19. Kaylar, L., "Experimentelle und theoretische Untersuchungen über den Einflub des Turbulenzgrades auf den Wärmeübergang in der Umgebung des Staupunktes eines Kreiszylinders," Forschung Ing.-Wes., Vol. 35, 1969, pp. 157-167.

20. Kestin, J., "The Effect of Free-Stream Turbulence on Heat Transfer Rates," Advances in Heat Transfer, Vol. 3, 1969, pp. 1-32.

21. Doebelin, E. O., "Generalized Performance Characteristics of Instruments," Ch. 3, Measurement Systems, Application and Design, 3rd Ed., McGraw-Hill Book Co., New York, 1983.

22. Torrance, K. E., "Numerical Methods in Heat Transfer," Ch. 5, Handbook of Heat Transfer, 2nd ed., edited by W. M. Rohsenow, J. P. Hartnet, and E. N. Ganic, McGraw-Hill Book Co., New York, 1985.

23. Anderson, D. A., Tannehill, J. C., and Pletcher, R. H., "Application of Finite-Difference Methods to Selected Model Equations," Ch. 4, Computational Fluid Mechanics and Heat Transfer, McGraw-Hill Book Co., New York, 1984.

APPENDIX A

LONGITUDINAL TEMPERATURE VARIATION OF TEST CYLINDER

One of the reasons for the wide dispersion in the published experimental results for convective heat transfer to bare cylinders can be attributed to heat conduction to the supports [7]. For negligible conduction losses, the aspect ratio (L/D) should be sufficiently large. Morgan [7] has reported that for a cylinder without heated end guard sections, the temperature is uniform over at least the center third of the cylinder when $L/D > 200$, but that in some experimental investigations this ratio has been less than 10. Since the aspect ratio of the test cylinder used in this experiment was 26, the validity of assuming uniform temperature over the center third of the cylinder had to be verified.

Knowing that the circumferential temperature variation over the test cylinder was negligible (Appendix B), a two-dimensional finite volume numerical approach [22] was used to calculate the steady state temperature distribution of the test cylinder. Because of symmetry only half of the length of the cylinder was analyzed. The stainless steel support was assumed to be a cylinder with the same diameter as the test cylinder, exchanging heat with the surroundings along its circumference, and having its temperature at one end maintained at the free stream temperature. The geometry was discretized into an array of 8 radial and 13 axial nodes, as shown in Figure A1. Radial and axial conductances were calculated [22] using:

$$C = kA/\ell \tag{A.1}$$

where

k = thermal conductivity

A = area of conduction

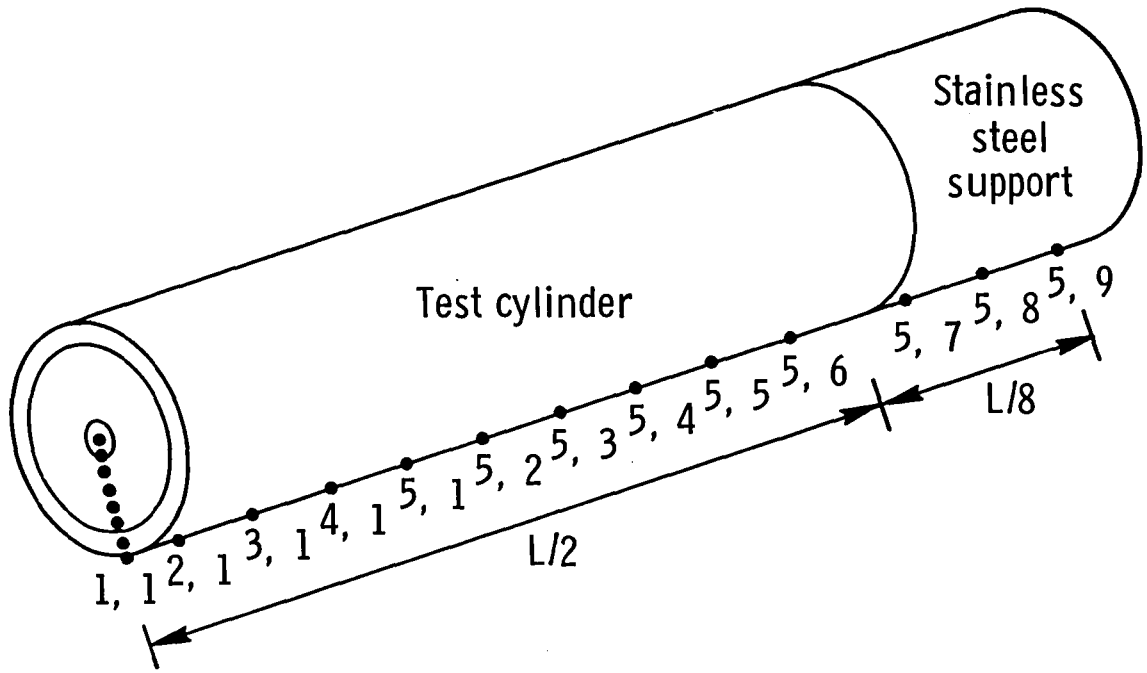

Fig. A1. Discretization of test cylinder for longitudinal temperature distribution analysis.

ℓ = length between nodes

The interface conductivities were calculated using

$$k = \frac{2k_i\, k_{i+1}}{k_i + k_{i+1}} \qquad (A.2)$$

since the interfaces were placed midway between nodes [22].

The thermal problem was solved using the Gauss-Seidel iteration with successive over relaxation [23] for both the lowest and highest Reynolds numbers used in the experiment -- 1,800 and 14,000. The longitudinal variation of nondimensionalized surface temperature with respect to the temperature gradient between the average surface temperature and free stream temperature for the two cases under consideration are shown in Figure A2. It can be seen that the surface temperature along the center third of the cylinder is basically uniform. A listing of the utlized program is included here.

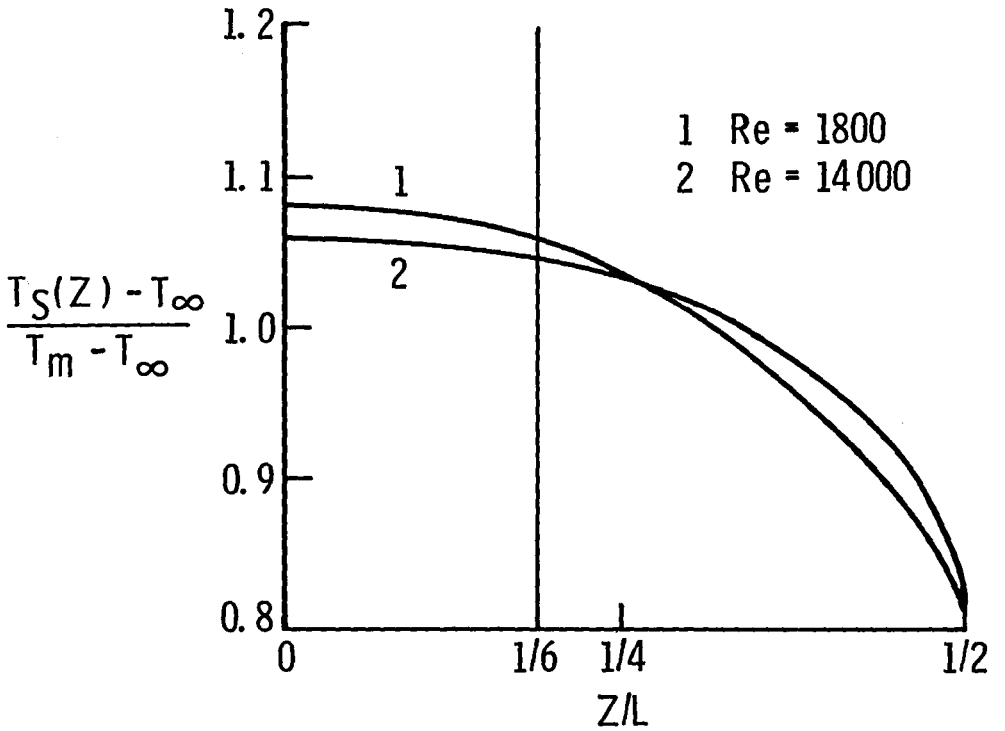

Fig. A2. Longitudinal variation of bare cylinder's surface temperature.

```
      PROGRAM T2          74/17   OPT=1,ROUND= A/ S/ M/-D,-DS      FTN 5.1+587        '86/04/11. 13.47.44
     DU=-LONG/-UT,ARG= COMMON/-FIXED,CS= USER/-FIXED,DB=-TB/-SB/-SL/-EP/-ID/-PMD/-ST,PL=50000
     FTN5,I=T31,PL.

 1                PROGRAM T2(INPUT,OUTPUT,TAPE3=OUTPUT)
 2                DIMENSION T(0:13,0:9),XY1(12,8),XY2(12,8),ERROR(12,8),TC(8),
 3               1CR(12,0:8),CZ(8,0:12),C(12,8),TCC(8),R(0:9),Z(13),DZ(12),ATC(8)
 4                M=12
 5                N=8
 6           C
 7           C
 8           C
 9           C
10           C  THIS PROGRAM WAS USED FOR CALCULATING THE STEADY STATE
11           C  TEMPERATURE DISTRIBUTION OF THE TEST CYLINDER, NEGLECTING
12           C  CIRCUMFERENTIAL TEMPERATURE VARIATION
13           C  THIS PROGRAM CONSISTS OF THE FOLLOWING STEPS:
14           C  -SPECIFICATION OF RADIAL & AXIAL NODE LOCATIONS
15           C  -CALCULATION OF  INTERFACE THERMAL CONDUCTIVITIES
16           C  -CALCULATION OF RADIAL & AXIAL CONDUCTANCES
17           C  -SOLUTION OF PROBLEM USING GAUSS-SEIDEL ITERATION WITH
18           C    SUCCESIVE OVER-RELAXATION
19           C
20           C  PARAMETERS USED HERE ARE:
21           C  RW = RADIUS OF HEATER WIRE
22           C  R(I) = RADIAL COORDINATES OF NODES
23           C  Z(J) = AXIAL COORDINATES OF NODES
24           C  DZ(J) = AXIAL NODAL DISTANCING
25           C  W = RELAXATION PRAMETER
26           C  E1 = CONVERGENCE CRITERIA
27           C  QL = HEAT GENERATION PER UNIT LENGTH
28           C  CK1 = THERMAL CONDUCTIVITY OF HEATER WIRE
29           C  CK2 = THERMAL CONDUCTIVITY OF POTTING COMPOUND
30           C  CK3 = THERMAL CONDUCTIVITY OF BRASS TUBE
31           C  CK4 = THERMAL CONDUCTIVITY OF STAINLESS STEEL SUPPORT
32           C  CH = COVECTIVE HEAT TRANSFER COEFFICIENT
33           C
34           C  TC(I) = RADIAL THERMAL CONDUCTIVITIES
35           C  TCC(J) = AXIAL THERMAL CONDUCTIVITIES
36           C  ATC(J) = AXIAL THERMAL CONDUCTIVITIES AT TUBE-SUPPORT
37           C             INTEPFACE
38           C  CR(I,J) = RADIAL CONDUCTANCES
39           C  CZ(I,J) = AXIAL  CONDUCTANCES
40           C  C(I,J)  = NODAL HEAT GENERATION TERMS
```

```
      C  T(I,J)  = NODAL TEMPERATURE (DIFFERENCE OF NODAL & FREE
      C               STREAM TEMPERATURES)
      C
      C
      C
      C  SPECIFICATION OF SOME PARAMETERS
      C
            PI=4.*ATAN(1.0)
            CK1=19.
            CK2=0.52
            CK3=111.
            CK4=14.4
            W=1.5
            E1=1.0E-5
            QL=26.0
      C
            X=25.4E-3
            RW=.020*X
            D1=0.010*X
            D2=0.021*X
            D3=.404*X
            D4=.399*X
            CH=70.
      C
      C
      C  SPECIFICATION OF RADIAL NODAL COORDINATES
      C
            R(0)=0.
            R(1)=0.0
            R(2)=D1
            R(3)=R(2)+2.0*D1
            DO 1 I=4,6
            R(I)=R(I-1)+D2
       1    CONTINUE
            R(7)=R(6)+2.0*D2
            R(8)=R(7)+D2
            R(9)=R(8)
      C
      C
      C  SPECIFICATION OF AXIAL NODAL COORDINATES
      C
            Z(1)=0.
```

```
      DO 2 I=2,11
      Z(I)=Z(I-1)+D3
    2 CONTINUE
      DO 201 I=12,13
      Z(I)=Z(I-1)+D4
  201 CONTINUE
C
C
C  CALCULATION OF AXIAL NODAL SPACING
C
C
      DZ(1)=0.5*(Z(2)-Z(1))
      DO 3 I=2,10
      DZ(I)=D3
    3 CONTINUE
      DZ(11)=(D3+D4)/2.
      DZ(12)=D4
C
C
C  CALCULATION OF AXIAL & RADIAL THERMAL CONDUCTIVITIES
C
C
      AA1=2.0*CK1*CK4/(CK1+CK4)
      AA2=2.0*CK2*CK4/(CK2+CK4)
      AA3=2.0*CK3*CK4/(CK3+CK4)
      DO 501 I=1,2
      ATC(I)=AA1
  501 CONTINUE
      DO 502 I=3,6
      ATC(I)=AA2
  502 CONTINUE
      DO 503 I=7,8
      ATC(I)=AA3
  503 CONTINUE
C
C
      TC(1)=CK1
      TC(2)=2.0*CK1*CK2/(CK1+CK2)
      DO 4 I=3,5
      TC(I)=CK2
    4 CONTINUE
      TC(6)=2.0*CK2*CK3/(CK2+CK3)
```

```
125                TC(7)=CK3
126           C
127                TCC(1)=CK1
128                TCC(2)=CK1
129                DO 5 I=3,6
130                TCC(I)=CK2
131            5   CONTINUE
132                DO 6 I=7,8
133                TCC(I)=CK3
134            6   CONTINUE
135           C
136           C
137           C  CALCULATION OF RADIAL CONDUCTANCES
138           C
139           C
140                DO 7 I=1,10
141                CR(I,8)=2.*PI*CH*R(8)*DZ(I)
142            7   CONTINUE
143                DO 8 I=1,10
144                DO 9 J=1,7
145                CR(I,J)=PI*TC(J)*DZ(I)*(R(J+1)+R(J))/(R(J+1)-R(J))
146            9   CONTINUE
147            8   CONTINUE
148                DO 511 I=11,12
149                DO 512 J=1,7
150                CR(I,J)=PI*CK4*DZ(I)*(R(J+1)+R(J))/(R(J+1)-R(J))
151            512 CONTINUE
152            511 CONTINUE
153                DO 513 I=11,12
154                CR(I,8)=2.*PI*CH*R(8)*DZ(I)
155            513 CONTINUE
156           C
157           C
158           C
159           C  CALCULATION OF AXIAL CONDUCTANCES
160           C
161           C
162                DO 10 I=1,8
163                B1=.25*PI*TCC(I)/D3*((R(I)+R(I+1))**2.0-(R(I)+R(I-1))**2.0)
164                DO 11 J=1,9
165                CZ(I,J)=B1
166            11  CONTINUE
```

```
      10   CONTINUE
           DO 514 I=1,8
           CZ(I,10)=.25*PI*ATC(I)/D3*((R(I)+R(I+1))**2.0-(R(I)+R(I-1))**2.0)
      514  CONTINUE
           DO 515 I=1,8
           BV=.25*PI*CK4/D4*((R(I)+R(I+1))**2.0-(R(I)+R(I-1))**2.0)
           DO 516 J=11,12
           CZ(I,J)=BV
      516  CONTINUE
      515  CONTINUE
C
C
C
C  CALCULATION OF NODAL HEAT GENERATION TERMS
C
C
           DO 44 I=1,M
           DO 45 J=1,N
           C(I,J)=0.0
      45   CONTINUE
      44   CONTINUE
C
           B3=QL*(0.5*R(2)/RW)**2.0
           B4=QL*(1-(0.5*R(2)/RW)**2.0)
           DO 13 I=1,10
           C(I,1)=B3*DZ(I)
           C(I,2)=B4*DZ(I)
      13   CONTINUE
C
C
C  INITIALIZING THE PROBLEM FOR GAUSS-SEIDEL PROCEDURE
C
           DO 14 I=1,M
           CR(I,0)=0.
           T(I,0)=1.
           T(I,9)=0.
      14   CONTINUE
           DO 15 J=1,8
           T(0,J)=1.
           CZ(J,0)=0.
           T(13,J)=0.
      15   CONTINUE
```

```
      C
            DO 18 I=1,M
            DO 16 J=1,N
            T(I,J)=0.0
            XY1(I,J)=0.0
       16   CONTINUE
       18   CONTINUE
      C
      C
      C
      C  SOLUTION OF PROBLEM USING GAUSS-SEIDEL ITERATION
      C  WITH SUCCESSIVE OVER-RELAXATION
      C
      C
            DO 200 K=1,50000
      C
            DO 20 I=1,M
            DO 21 J=1,N
            T(I,J)=(C(I,J)+CR(I,J-1)*T(I,J-1)+CR(I,J)*T(I,J+1)+CZ(J,I)*
           1T(I+1,J)+CZ(J,I-1)*T(I-1,J))/(CR(I,J-1)+CR(I,J)+CZ(J,I)+CZ(J,I-1))
            XY2(I,J)=T(I,J)
       21   CONTINUE
       20   CONTINUE
      C
            DO 25 I=1,M
            DO 26 J=1,N
            ERROR(I,J)=ABS(XY2(I,J)-XY1(I,J))
            IF(ERROR(I,J).GT.E1) THEN
1             GO TO 71
            ELSE
1             IF(I.EQ.M.AND.J.EQ.N) THEN
2               GO TO 70
2             ELSE
2               GO TO 26
2             END IF
1           END IF
       26   CONTINUE
       25   CONTINUE
       71   CONTINUE
            DO 27 I=1,M
            DO 28 J=1,N
            XY1(I,J)=XY1(I,J)+W*(XY2(I,J)-XY1(I,J))
```

```
      PROGRAM T2          74/17   OPT=1,ROUND= A/ S/ M/-D,-DS     FTN 5.1+587        86/04/11. 13.47.44

251                       T(I,J)=XY1(I,J)
252                 28    CONTINUE
253                 27    CONTINUE
254                 200   CONTINUE
255                       WRITE(3,60)
256                 60    FORMAT (3X,' NOT CONVERGING')
257                       GO TO 80
258                 70    CONTINUE
259                       DO 29 I=1,M
260                       DO 30 J=1,N
261                       WRITE(3,61) I,J,T(I,J)
262                 61    FORMAT(3X,'T(',I2,',',I2,')=',3X,F8.3)
263                 30    CONTINUE
264                 29    CONTINUE
265                 80    STOP
266                       END
```

APPENDIX B

CIRCUMFERENTIAL TEMPERATURE VARIATION OF TEST CYLINDER

Local heat transfer coefficient on a circular cylinder varies considerably across the surface of the cylinder [9]. This would in turn cause circumferential variation of surface temperature around the cylinder. Even though a relatively high thermal conductivity tube (brass) was utilized to prevent significant surface temperature variation, further analytical investigation was required to determine maximum steady state surface temperature variation for the bare cylinder. A two-dimensional finite volume numerical analysis [22] of the test cylinder was utilized for this purpose. The geometry was discretized into an array of 8 radial nodes and 7 circumferential nodes, as shown in Figure B1. The radial and circumferential conductances, and the interface thermal conductivities were calculated as prescribed in Appendix A. Schmidt and Wenner's [9] data for the circumferential variation of Nusselt number for a Reynolds number of 39,800, shown in Figure 10, was used in this study.

The thermal problem was solved using the Gauss-Seidel iteration with successive over relaxation [23]. It was found that the maximum circumferential temperature variation would be 0.03°C for the considered case. A listing of the utilized program is given here.

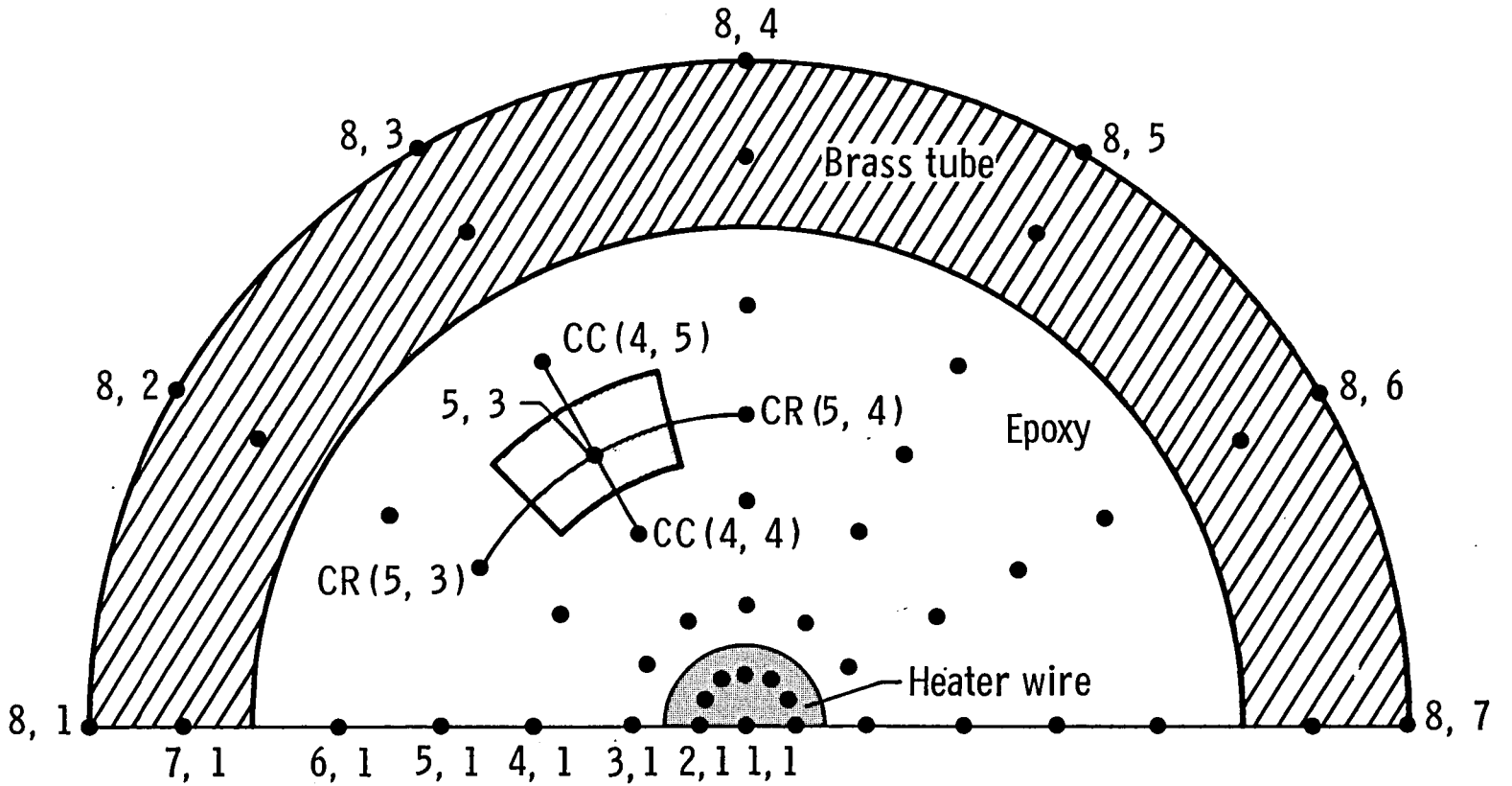

Fig. B1. Discretization of test cylinder for circumferential temperature distribution analysis.

```
    PROGRAM T1          74/17   OPT=1,ROUND= A/ S/ M/-D,-DS      FTN 5.1+587          86/05/01. 19.52.34
DB=-LONG/-DT,ARG= COMMON/-FIXED,CS= USER/-FIXED,DB=-TB/-SB/-SL/-ER/-ID/-PMD/-ST,PL=50000
+INS,I=T1,PL.

  1                 PROGRAM T1(INPUT,OUTPUT,TAPE3=OUTPUT)
  2                 DIMENSION T(8,7),XY1(8,7),XY2(8,7),ERROR(8,7),TC(8),TCC(8),R(8)
  3                1,RC(9,7),CC(8,7),C(8,7),CH(7)
  4                 M=8
  5                 N=7
  6           C
  7           C
  8           C
  9           C
 10           C  THIS PROGRAM WAS USED FOR CALCULATING THE STEADY STATE
 11           C  TEMPERATURE DISTRIBUTION OF THE TEST CYLINDER, NEGLECTING
 12           C  AXIAL TEMPERATURE VARIATION
 13           C  THIS PROGRAM CONSISTS OF THE FOLLOWING STEPS:
 14           C  -SPECIFICATION OF RADIAL & CIRCUMFERENTIAL NODE LOCATIONS
 15           C  -CALCULATION OF INTERFACE THERMAL CONDUCTIVITIES
 16           C  -CALCULATION OF RADIAL & CIRCUMFERENTIAL CONDUCTANCES
 17           C  -SOLUTION OF PROBLEM USING GAUSS-SEIDEL ITERATION WITH
 18           C    SUCCESIVE OVER-RELAXATION
 19           C
 20           C  PARAMETERS USED HERE ARE:
 21           C  RW = RADIUS OF HEATER WIRE
 22           C  R(I) = RADIAL COORDINATES OF NODES
 23           C  DT = CIRCUMFERENTIAL DISTANCING
 24           C  W = RELAXATION PARAMETER
 25           C  E1 = CONVERGENCE CRITERIA
 26           C  QL = HEAT GENERATION PER UNIT LENGTH
 27           C  CK1 = THERMAL CONDUCTIVITY OF HEATER WIRE
 28           C  CK2 = THERMAL CONDUCTIVITY OF POTTING COMPOUND
 29           C  CK3 = THERMAL CONDUCTIVITY OF BRASS TUBE
 30           C  TC(I) = RADIAL THERMAL CONDUCTIVITIES
 31           C  TCC(I) = CIRCUMFERENTIAL THERMAL CONDUCTIVITIES
 32           C  CH(I) = CONVECTIVE HEAT TRANSFER COEFFICIENTS
 33           C  RC(I,J) = RADIAL CONDUCTANCES
 34           C  CC(I,J) = CIRCUMFERENTIAL CONDUCTANCES
 35           C  C(I,J) = NODAL HEAT GENERATION TERMS
 36           C  T(I,J) = NODAL TEMPERATURES (DIFFERENCE OF NODAL & FREE
 37           C              STREAM TEMPERATURES)
 38           C
 39           C
 40           C
```

```
      PROGRAM TI          74/17   OPT=1,ROUND= A/ S/ M/-D,-DS      FTN 5.1+587          86/05/01. 19.52.34

      C
      C
      C  SPECIFICATION OF PARAMETERS
      C
      C
            PI=4.*ATAN(1.0)
            DT=PI/6.0
            CK1=19.
            CK2=0.52
            CK3=111.
            K=1.5
            E1=1.0E-6
            QL=26.0
      C
            X=25.4E-3
            RW=.020*X
            D1=0.010*X
            D2=0.021*X
      C
      C  SPECIFICATION OF RADIAL NODAL COORDINATES
      C
            R(1)=0.0
            R(2)=D1
            R(3)=R(2)+2.0*D1
            DO 100 I=4,6
            R(I)=R(I-1)+D2
  100       CONTINUE
            R(7)=R(6)+2.0*D2
            R(8)=R(7)+D2
      C
      C
      C  SPECIFICATION OF CONVECTIVE HEAT TRANSFER COEFFICIENTS
      C    FROM SCHMIDT & WENNER'S DATA [9]
      C
            CH(1)=655.
            CH(2)=590.
            CH(3)=393.
            CH(4)=164.
            CH(5)=327.
            CH(6)=455.
            CH(7)=655.
      C
```

```
      C
      C  CALCULATION OF RADIAL THERMAL CONDUCTIVITIES
      C
            TC(2)=CK1
            TC(3)=2.0*CK1*CK2/(CK1+CK2)
            DO 1 I=4,6
            TC(I)=CK2
    1       CONTINUE
            TC(7)=2.0*CK2*CK3/(CK2+CK3)
            TC(8)=CK3
      C
      C
      C  CALCULATION OF CIRCUMFERENTIAL THERMAL CONDUCTIVITIES
      C
            TCC(2)=CK1
            DO 2 I=3,6
            TCC(I)=CK2
    2       CONTINUE
            DO 3 I=7,8
            TCC(I)=CK3
    3       CONTINUE
      C
      C
      C
      C  CALCULATION OF RADIAL CONDUCTANCES
      C
      C
            B1=0.25*TC(2)*DT
            RC(2,1)=B1
            RC(2,7)=B1
            DO 4 I=2,6
            RC(2,I)=2.0*B1
    4       CONTINUE
            DO 5 I=3,6
            B2=0.25*TC(I)*(R(I)+R(I-1))/(R(I)-R(I-1))*DT
            DO 6 J=1,7
            IF(J.EQ.1.AND.J.EQ.7) THEN
              RC(I,J)=B2
            ELSE
              RC(I,J)=2.0*B2
            END IF
    6       CONTINUE
```

```
125             5     CONTINUE
126                   FC(9,1)=CH(1)*R(6)*DT/2.0
127                   FC(9,7)=CH(7)*R(8)*DT/2.0
128                   DO 7 I=2,6
129                   FC(9,I)=CH(I)*R(8)*DT
130             7     CONTINUE
131           C
132           C
133           C
134           C
135           C  CALCULATION OF CIRCUMFERENTIAL CONDUCTANCES
136           C
137           C
138                   B3=TCC(2)*R(3)/(R(2)*DT)
139                   DO 8 I=2,7
140                   CC(2,I)=0.5*B3
141             8     CONTINUE
142           C
143                   DO 9 I=3,7
144                   B4=TCC(I)*(R(I+1)+R(I-1))/(R(I)*DT)
145                   DO 10 J=2,7
146                   CC(I,J)=0.50*B4
147            10     CONTINUE
148             9     CONTINUE
149           C
150                   B5=TCC(8)*(R(6)-R(7))/(R(8)*DT)
151                   DO 11 I=2,7
152                   CC(6,I)=0.5*B5
153            11     CONTINUE
154           C
155           C
156           C
157           C
158           C
159           C  CALCULATION OF NODAL HEAT GENERATION TERMS
160           C
161                   DO 12 I=1,M
162                   DO 13 J=1,N
163                   C(I,J)=0.0
164            13     CONTINUE
165            12     CONTINUE
166                   QHG=QL/(RW**2.0)
```

```
      C(1,1)=EHG*(R(2)/2.)**2.
      BB=EHG*(RW**2.-(R(2)/2.)**2.)/6.
      C(2,1)=0.5*BB
      C(2,7)=0.5*BB
      DO 14 I=2,6
      C(2,I)=BB
   14 CONTINUE
C
C
C
C  PROVIDING INITIAL GUESS FOR TEMPERATURE DISTRIBUTION
C
      DO 15 I=1,M
      DO 16 J=1,N
      T(I,J)=0.0
      XY1(I,J)=0.0
   16 CONTINUE
   15 CONTINUE
C
C
C
C  SOLUTION OF THE PROBLEM USING GUASS-SEIDEL ITERATION
C   WITH SUCCESIVE OVER-RELAXATION
C
      DO 200 K=1,10000
      Z=RC(2,1)+RC(2,2)+RC(2,3)+RC(2,4)+RC(2,5)+RC(2,6)+RC(2,7)
      T(1,1)=1./Z*(C(1,1)+RC(2,1)*T(2,1)+RC(2,2)*T(2,2)+RC(2,3)*T(2,3)+
     1RC(2,4)*T(2,4)+RC(2,5)*T(2,5)+RC(2,6)*T(2,6)+RC(2,7)*T(2,7))
      I=2
      DO 16 J=1,7
      IF(J.EQ.1) THEN
        T(I,J)=(C(I,J)+RC(1,J)*T(1,1)+RC(I+1,J)*T(I+1,J)+CC(I,J+1)*
     1  T(I,J+1))/(RC(I,J)+RC(I+1,J)+CC(I,J+1))
      ELSE
        IF(J.EQ.7) THEN
          T(I,J)=(C(1,J)+RC(I,J)*T(1,1)+RC(1+1,J)*T(I+1,J)+CC(I,J)*
     1    T(I,J-1))/(RC(I,J)+RC(I+1,J)+CC(1,J))
        ELSE
          T(I,J)=(C(1,J)+RC(I,J)*T(1,1)+RC(1+1,J)*T(I+1,J)+
     1    CC(I,J)*T(I,J-1)+CC(1,J+1)*T(I,J+1))/(RC(I,J)+RC(I+1,J)+
     1    CC(1,J)+CC(1,J+1))
        END IF
```

```
1    209                 END IF
     210           18    CONTINUE
     211                 C
     212                 DO 19 I=3,7
     213                 DO 20 J=1,7
     214                 IF(J.EQ.1) THEN
1    215                   T(I,J)=(C(I,J)+RC(I,J)*T(I-1,J)+RC(I+1,J)*T(I+1,J)+
1    216                1  CC(I,J+1)*T(I,J+1))/(RC(I,J)+RC(I+1,J)+CC(I,J+1))
1    217                 ELSE
1    218                   IF(J.EQ.7) THEN
2    219                     T(I,J)=(C(I,J)+RC(I,J)*T(I-1,J)+RC(I+1,J)*T(I+1,J)+
2    220                1    CC(I,J)*T(I,J-1))/(RC(I,J)+RC(I+1,J)+CC(I,J))
2    221                   ELSE
2    222                     T(I,J)=(C(I,J)+RC(I,J)*T(I-1,J)+RC(I+1,J)*T(I+1,J)+
2    223                1    CC(I,J)*T(I,J-1)+CC(I,J+1)*T(I,J+1))/(RC(I,J)+
2    224                1    RC(I+1,J)+CC(I,J)+CC(I,J+1))
2    225                   END IF
1    226                 END IF
     227           20    CONTINUE
     228           19    CONTINUE
     229                 C
     230                 I=8
     231                 DO 21 J=1,7
     232                 IF(J.EQ.1) THEN
1    233                   T(I,J)=(C(I,J)+RC(I,J)*T(I-1,J)+CC(I,J+1)*T(I,J+1))/(RC(I,J)+
1    234                1  RC(I+1,J)+CC(I,J+1))
1    235                 ELSE
1    236                   IF(J.EQ.7) THEN
2    237                     T(I,J)=(C(I,J)+RC(I,J)*T(I-1,J)+CC(I,J)*T(I,J-1))/(RC(I,J)+
2    238                1    RC(I+1,J)+CC(I,J))
2    239                   ELSE
2    240                     T(I,J)=(C(I,J)+RC(I,J)*T(I-1,J)+CC(I,J)*T(I,J-1)+CC(I,J+1)*
2    241                1    T(I,J+1))/(RC(I,J)+RC(I+1,J)+CC(I,J)+CC(I,J+1))
2    242                   END IF
1    243                 END IF
     244           21    CONTINUE
     245                 C
     246                 DO 23 I=1,M
     247                 DO 24 J=1,N
     248                 XY2(I,J)=T(I,J)
     249           24    CONTINUE
     250           23    CONTINUE
```

```
PROGRAM T1          74/17   OPT=1,ROUND=A/S/M/-D,-DS      FTN 5.1+587        86/05/01. 19.52.34

                      DO 25 I=1,M
                      DO 26 J=1,N
                      ERROR(I,J)=ABS(XY2(I,J)-XY1(I,J))
                      IF(ERROR(I,J).GT.E1) THEN
                        GO TO 71
                      ELSE
                        IF(I.EQ.M.AND.J.EQ.N) THEN
                          GO TO 70
                        ELSE
                          GO TO 26
                        END IF
                      END IF
                26    CONTINUE
                25    CONTINUE
                71    CONTINUE
                      DO 27 I=1,M
                      DO 28 J=1,N
                      XY1(I,J)=XY2(I,J)+W*(XY2(I,J)-XY1(I,J))
                      T(I,J)=XY1(I,J)
                28    CONTINUE
                27    CONTINUE
                200   CONTINUE
                      WRITE(3,60)
                60    FORMAT (3X,' NOT CONVERGING')
                      GO TO 80
                70    CONTINUE
                      DO 29 I=1,M
                      DO 30 J=1,N
                      WRITE(3,61) I,J,T(I,J)
                61    FORMAT(3X,'T(',I2,',',I2,')=',3X,F6.3)
                30    CONTINUE
                29    CONTINUE
                80    STOP
                      END
```

APPENDIX C

RADIATION CORRECTION FOR BARE CYLINDER

The bare cylinder exchanges radiant energy with the wind tunnel walls as shown in Figure C.1. The bare cylinder is designated as surface 1, and wind tunnel walls are designated as surfaces 2 and 4. Surfaces 3 and 4 are imaginary surfaces -- at free-stream temperature -- for completing the enclosure. The formulation is based on the assumption of radiant exchange between gray surfaces through non-participating media.

The net radiant heat flux for each of the surfaces can be obtained from:

$$(\overset{"}{q}_i)_{net} = J_i - G_i \tag{C.1}$$

The irradiation, G, on each surface is due to energy leaving that surface (if it can "see" itself) and the other surfaces:

$$A_i G_i = \sum_j A_j F_{j-i} J_j \tag{C.2}$$

Applying reciprocity to this equation yields:

$$G_i = \sum_j F_{i-j} J_j \tag{C.3}$$

The radiosity, J, is the sum of the emitted energy and reflected irradiation, and can be calculated according to:

$$J_i = \varepsilon_i E_{b,i} + (1 - \varepsilon_i) G_i \tag{C.4}$$

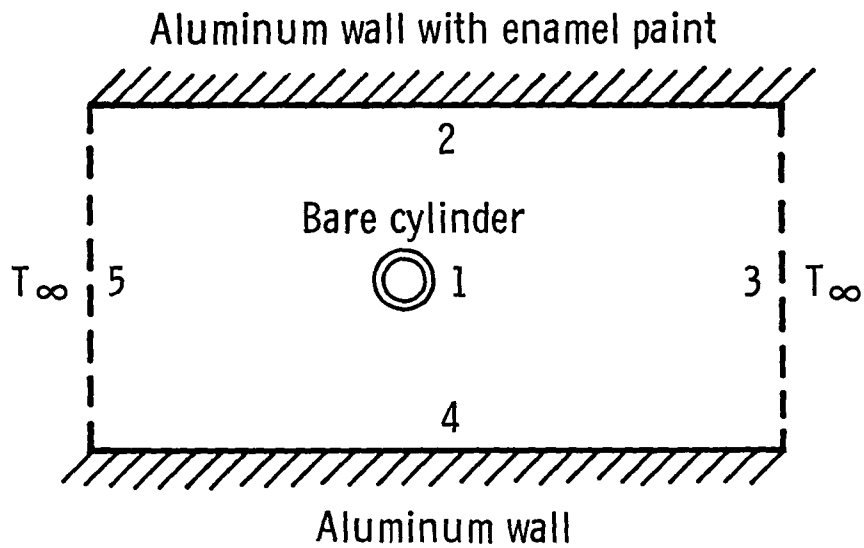

Fig. C1. Schematic diagram for radiation heat flux correction for bare cylinder case.

Combining Equations C.1, C.3, and C.4 results in

$$(q_i'')_{net} = \frac{-\varepsilon_i}{1-\varepsilon_i} (J_i - E_{b,i}) \qquad (C.5)$$

The radiosity for surface 1 can be calculated according to

$$J_1 = \varepsilon\ \sigma\ T_s^4 + (1-\varepsilon)\ [F_{1-2}\ J_2 + F_{1-3'},\ R_{3'} + F_{1-4}\ R_4] \qquad (C.6)$$

where surface 3' is the combination of surfaces 3 and 5.

The radiosities for the other surfaces are:

$$J_{3'} = \sigma T_\infty^4 \qquad \text{(black body assumption)} \qquad (C.7)$$

$$J_2 = \varepsilon_2 \sigma T_w^4 + (1-\varepsilon_2)\ [F_{2-1} J_1 + F_{2-3'}\ J_{3'} + F_{2-4}\ J_4] \qquad (C.8)$$

$$J_4 = \varepsilon_4 \sigma T_w^4 + (1-\varepsilon_4)\ [F_{4-1} J_1 + F_{4-2}\ J_2 + F_{4-3'}\ J_{3'}] \qquad (C.9)$$

Combining Equations C.5 through C.9 results in

$$q_{R1}'' = (q_1'')_{net} = -\ 0.562\ \sigma[0.430\ T_\infty^4 + 0.215\ T_w^4 - 0.639\ T_s^4] \qquad (C.10)$$

where, crossed-string method [12] has been used to calculate the shape factors (F_{i-j}), and the following total normal emissivities have been used:

$\varepsilon = .36$

$\varepsilon_2 = 0.9$ (enamel paint) [12]

$\varepsilon_3 = 0.07$ (aluminum, rough plate) [12]

Equation C.10 was used for calculating the radiation heat flux corrections for the bare cylinder case.

1. Report No.	2. Government Accession No.	3. Recipient's Catalog No.
NASA CR-4005		

4. Title and Subtitle	5. Report Date
Convective Heat Transfer From Circular Cylinders Located Within Perforated Cylindrical Shrouds	August 1986
	6. Performing Organization Code
7. Author(s)	8. Performing Organization Report No.
Kamran Daryabeigi and Robert L. Ash	
	10. Work Unit No.
9. Performing Organization Name and Address Old Dominion University Research Foundation P. O. Box 6369 Norfolk, Virginia 23508	11. Contract or Grant No. NAS1-17993 T.A. No. 23
	13. Type of Report and Period Covered Contractor Report 10/16/85-09/30/86
12. Sponsoring Agency Name and Address National Aeronautics and Space Administration Washington, D.C. 20546-0001	14. Sponsoring Agency Code 505-61-01-05

15. Supplementary Notes

Langley Technical Monitor: L. A. Dillon-Townes
Principal Investigator: Dr. Robert L. Ash

16. Abstract

The influence of perforated cylindrical shrouds on the convective heat transfer to circular cylinders in transverse flow has been studied experimentally. Geometries studied were similar to those used in industrial platinum resistance thermometers. The influence of Reynolds number, ventilation factor (ratio of the open area to the total surface area of shroud), radius ratio (ratio of shroud's inside radius to bare cylinder's radius), and shroud orientation with respect to flow were studied.

The experiments showed that perforated shrouds with ventilation factors in the range 0.1 to 0.4 and radius ratios in the range 1.1 to 2.1 could enhance the convective heat transfer to bare cylinders up to 50%. The maximum enhancement occurred for a radius ratio of 1.4 and ventilation factors between 0.2 and 0.3. It was found that shroud orientation influenced the heat transfer, with maximum heat transfer generally occurring when the shroud's holes were centered on either side of the stagnation line. However, the hole orientation effect is of second order compared to the influence of ventilation factor and radius ratio.

17. Key Words (Suggested by Author(s))	18. Distribution Statement
Convective heat transfer Perforated shrouds Platinum resistance thermometry	Unclassified - Unlimited Subject category 34

19. Security Classif. (of this report)	20. Security Classif. (of this page)	21. No. of Pages	22. Price*
Unclassified	Unclassified	102	A06

* For sale by the National Technical Information Service, Springfield, Virginia 22161

NASA-Langley, 1986

End of Document